Spectrochimica Acta Part A: Molecular and Biomolecular Spectroscopy 175 (2017) 76–91

Contents lists available at ScienceDirect

Spectrochimica Acta Part A: Molecular and Biomolecular Spectroscopy

journal homepage: www.elsevier.com/locate/saa

Synthesis, structure, spectral properties and DFT quantum chemical calculations of 4-aminoazobenzene dyes. Effect of intramolecular hydrogen bonding on photoisomerization

Anton Georgiev [a,*], Emil Bubev [a], Deyan Dimov [b], Denitsa Yancheva [c], Ivaylo Zhivkov [b,d], Jozef Krajčovič [d], Martin Vala [d], Martin Weiter [d], Maria Machkova [a]

[a] Department of Organic and Physical Chemistry, 1756 Sofia, 8 St. Kliment Ohridski Blvd, University of Chemical Technology and Metallurgy, Bulgaria
[b] Department of Nanostructured Materials and Technology, 1113, Sofia, 109 Acad. G. Bonchev Blvd, Institute of Optical Materials and Technologies, Bulgarian Academy of Science, Bulgaria
[c] Laboratory of Structural Organic Analysis, Sofia 1113, 9 Acad. G. Bonchev Blvd, Institute of Organic Chemistry with Centre of Phytochemistry, Bulgarian Academy of Science, Bulgaria
[d] Materials Research Centre, Faculty of Chemistry, Purkyňova 118, Brno, Brno University of Technology, Czech Republic

ARTICLE INFO

Article history:
Received 30 October 2016
Received in revised form 27 November 2016
Accepted 7 December 2016
Available online 09 December 2016

Keywords:
4-aminoazobenzene dyes
DFT quantum chemical calculations
HOMO and LUMO energy levels
Solvatochromism
Photoisomerization
UV-VIS spectroscopy

ABSTRACT

In this paper three different "push-pull" 4-aminoazobenzene dyes have been synthesized in order to characterize their photochromic behavior in different solvents. The molecular geometry was optimized by DFT/B3LYP functional combined with the standard 6–31 + G(d,p) basis set for *trans (E)* and *cis (Z)* isomers and the energy levels of HOMO and LUMO frontier orbitals were computed using IEFPCM solvation in $CHCl_3$ and DMF. The calculated results were compared to the experimental optical band gap and HOMO values of cyclic voltammetry. The intramolecular six-membered hydrogen bond was formed in both isomers of the synthesized dyes. The thermodynamic parameters such as total electronic energy *E (RB3LYP)*, enthalpy H_{298} (sum of electronic and thermal enthalpies), free Gibbs energy G_{298} (sum of electronic and thermal free Gibbs energies) and dipole moment μ were computed for *trans (E)* and *cis (Z)* isomers in order to estimate the $\Delta E_{trans \rightarrow cis}$, $\Delta\mu_{trans \rightarrow cis}$, $\Delta H_{trans \rightarrow cis}$, $\Delta G_{trans \rightarrow cis}$ and $\Delta S_{trans \rightarrow cis}$ values. The NBO analysis was performed in order to understand the intramolecular charge transfer and energy of resonance stabilization. The solvatochromic shift was evaluated by UV-VIS spectroscopy in $CHCl_3$ (nonpolar), EtOH (polar protic) and DMF (polar aprotic) solvents to determine the electron withdrawing and donating properties of the substituents on electron transitions energy. Through the increasing solvent polarity a strong bathochromic shift is observed. The photoisomerization experiments have been performed in two solvents $CHCl_3$ (nonpolar) and DMF (polar aprotic) by UV light irradiation with $\lambda = 365$ nm at equal concentrations and time of illuminations. The electronic spectra were computed by TD-DFT after geometry optimization using IEFPCM solvation in $CHCl_3$ and DMF. The degree of photoisomerization was calculated for the three azo chromophores in both solvents. By using first derivative of the UV-VIS spectra it was possible to resolve the overlapped electron transitions absorption bands. The existing intramolecular hydrogen bond in the azo chromophores was discussed in relation to the isomerization mechanisms and relative stability of the *cis (Z)* isomers.

1. Introduction

Azobenzene derivatives (ABs) contain chromophore —N=N— (azo) group, which undergoes reversible *trans-cis-trans* photoisomerization cycle. The main characteristic UV-VIS absorption bands are at λ_{max} ~ 440 nm related to the n → π* transition or S_1 excited state and at λ_{max} ~ 340 nm related to the π → π* transition or S_2 excited state [1,2]. The *trans-cis* isomerization can be driven by ultraviolet (UV) light irradiation usually at λ ~ 365 nm, the reverse *cis-trans* isomerization occurs spontaneously in the dark, under thermal treatment or by exposure to visible (VIS) light. The *trans (E)* isomer is more thermodynamically stable than *cis (Z)* one due to higher energy of *cis (Z)* twist conformation related to the orbitals repulsion between aromatic rings and substituents [2,3]. Geometrically, the *cis*-ABs are characterized by 90° twisting of the aromatic rings relative to plane of the azo bond and 44% reduction in the distance between the 4 and 4′ positions: ~9 Å (*trans*) and ~5.5 Å (*cis*) [4]. Fig. 1 illustrates the photoisomerization of ABs and the potential energy levels of electron transitions on ground (singlet) state and first S_1 and second S_2 excited states.

According to the spectral properties, nature and position of the substituents in the aromatic rings azobenzene derivatives can be classified (by Rau) [5] as: (i) azobenzene derivatives (ABn); (ii) aminoazobenzene derivatives (aAB); (iii) pseudostilbenes (pSB).

* Corresponding author.
E-mail address: antonchem@abv.bg (A. Georgiev).

http://dx.doi.org/10.1016/j.saa.2016.12.005
1386-1425/

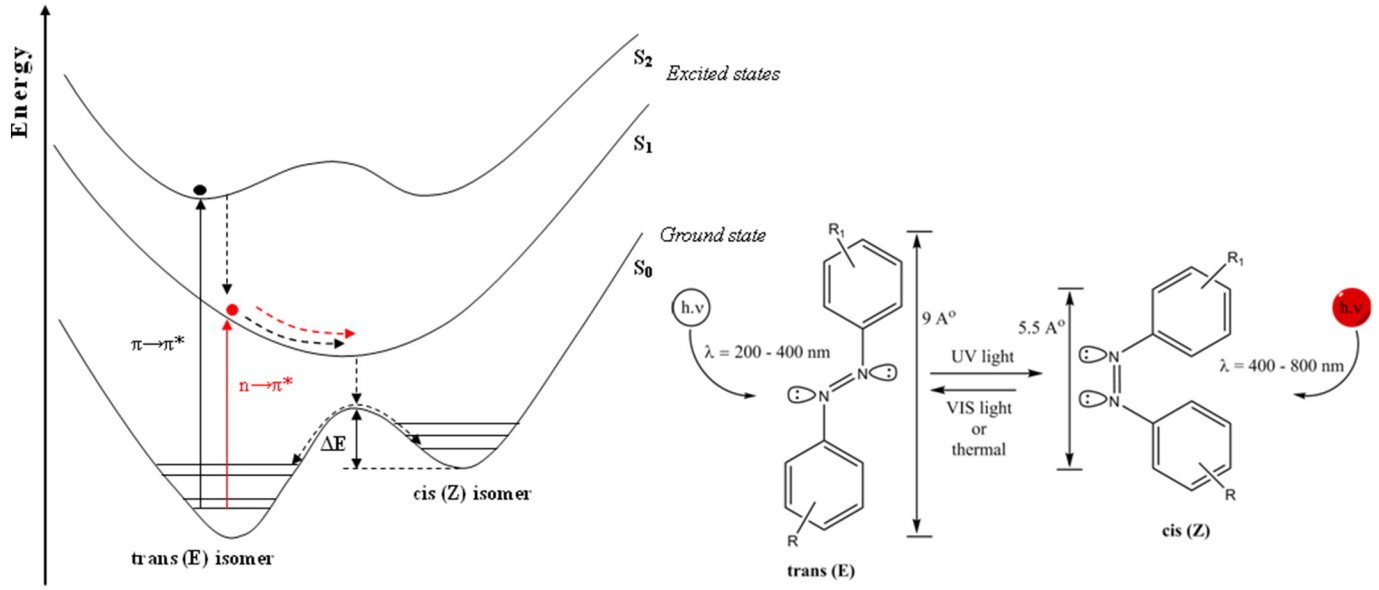

Fig. 1. Schematic representation of photoisomerization of the AB derivatives and the potential energy levels of ground (singlet) state and first S_1 and second S_2 excited states, adapted from Y. M. Riyad et al. [3].

Fig. 2 presents the nature and position of the functional groups in substituted ABs.

The substitution pattern of the AB molecules determines their photochemical behavior. Four mechanisms have been proposed in order to understand the photoisomerization pathway: (i) rotation; (ii) inversion; (iii) concerted inversion; (iv) inversion-assisted rotation. The rotational pathway involves rupture of the N ═N π-bond to allow free rotation about the N—N σ-bond. The rotation changes the C—N—N—C dihedral angle while the N═N—C angle remains fixed at ~120°. In the inversion mechanism, one N═N—C angle increases to 180° while the C—N═N—C dihedral angle remains fixed at 0°, where in a transition $S_0 \rightarrow S_1$ ($n \rightarrow \pi^*$) state leads to the inversion around one of nitrogen in the same molecular plane and excitation to the $S_0 \rightarrow S_2$ ($\pi \rightarrow \pi^*$) state provokes isomerization via rotation one of the phenyl ring around the N ═N double bond. For isomerization to occur by concerted inversion, both N═N—C bond angles increase to 180° generating a linear transition state. In inversion-assisted rotation, large changes in the C—N═N—C dihedral angle and smaller but significant changes in the N═N—C angles occur simultaneously [1,6,7]. The described mechanisms have been confirmed by quantum mechanical calculations and ultrafast time-resolved spectroscopy [8,9]. Multiple isomerization pathways have often been involved to explain experimental photochemical behavior.

Several factors are known to affect the photoisomerization: (i) The nature of the substituents in the aromatic rings. The presence of electron withdrawing (EW) groups like —CHO, —CN, —NO_2 decrease the energy of the electron transitions, where the $\pi \rightarrow \pi^*$ and $n \rightarrow \pi^*$ bands are well separated. (ii) The solvent properties are important for the photochromic behavior due to the dipole-dipole interaction with the azo dye molecules, leading to solvatochromic shifting. Nonpolar solvents weakly interact with the nonbonding electron pairs of the substituents and azo nitrogens, therefore they affect slightly the isomerization. However, the polar solvents (protic or aprotic) interact with the azo chromophores and a bathochromic shift (red shift) is observed related to the decrease of the electron transition energy. (iii) Intermolecular hydrogen bonds can be formed between two or more azo molecules or between the solvent and azo chromophores. The intramolecular hydrogen bonds can be formed as: a) proton transfer between azo nitrogens and

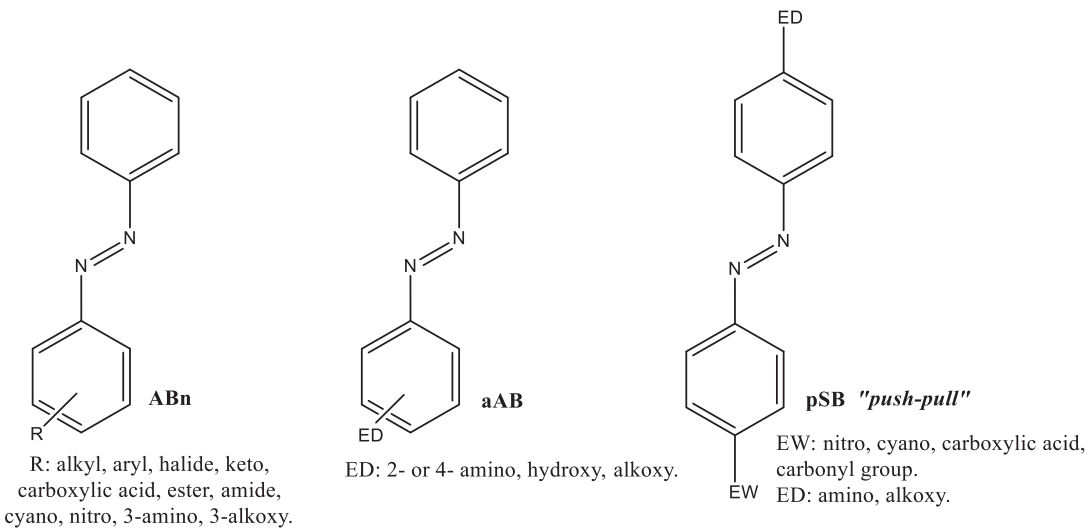

Fig. 2. General types of the substituted ABs.

ortho phenol hydroxyl (or other proton donors) group. In this case, the intramolecular hydrogen bonding or H-transfer depend on the solvent polarity, pH medium and electronic properties of the other substituents; b) polar interaction without proton transfer between azo nitrogens and *ortho* proton donors like —CH_2OH, —CH_2NH_2, where the intramolecular hydrogen bonds are not affected by the solvent properties. The properties and position of the substituents respect to the azo nitrogens strongly affect the photoisomerization, which change the energy of electron transitions. (iv) The irradiation wavelength applied for $\pi \rightarrow \pi^*$ ($S_0 \rightarrow S_2$) transitions in UV region is usually at $\lambda \sim 365$ nm, while for $n \rightarrow \pi^*$ ($S_0 \rightarrow S_1$) transitions in VIS range is approximately at $\lambda \sim 450–550$ nm. The intensity and time of irradiation influence the degree of isomerization. (ν) Higher temperature favors the *cis* → *trans* conversion, due to the thermodynamically more stable *trans (E)* isomer [1,10,11,12,13].

In previous reported works there are many useful quantum chemical calculations on azo chromophores in order to explain their spectral properties and molecular geometry [11,12,13,14,15]. By using the density-functional theory (DFT) with B3LYP hybrid functional the isomerization mechanisms have been proved for different types ABs. A. Mahmood et al. have compared the capability of B3LYP hybrid functional with four different basis set (6-31G, 6-31 + G, 6-31 + G* and 6-31 + G**) to predict the electron transitions spectra of several heterocyclic azo chromophores applied in dye sensitized solar cells (DSSCs). They have found that 6-31 + G and 6-31 + G* basis sets have good fit to the experimental data [14]. Six novel azo dyes with different π-spacers have been synthesized and investigated by S.B. Novir et al. through time dependent density-functional theory (TD-DFT) and DFT with B3LYP hybrid functional in order to predict π-conjugation effects, which are important for performance parameters of DSSCs [15]. The authors have found good agreement between theoretical and experimental results.

Azo-containing materials exhibit photoactive properties with potential application as optical photoswitches, reversible information storage, organic solar cells, bioengineering devices, nonlinear optical materials, polyelectrolyte multilayers, liquid crystals and other photoactive and photomechanical devices [2,4,16]. Photoinduced isomerization between *trans (E)* and *cis (Z)* isomers and the occurrence of magnetic anisotropy are the main properties of these compounds, which determine their practical applications. Therefore the aim of the present study was to synthesize and characterize the spectral properties of three "push-pull" 4-aminoazobenzene dyes *(E)-2-((4-Amino-2-(Hydroxymethyl)Phenyl)Diazenyl)-5-Nitrobenzonitrile* (Azo-1), *(E)-(5-Amino-2-((2.4-Dinitrophenyl)Diazenyl)Phenyl)Methanol* (Azo-2) and *(E)-(5-Amino-2-((4-Bromo-2-Methylphenyl)Diazenyl)Phenyl)Methanol* (Azo-3). The specific aims were: (i) synthesis, characterization and quantum chemical calculations by DFT/B3LYP functional combined with the standard 6–-31 + G(d,p) basis set of the synthesized azo dyes; (ii) experimental determination of HOMO and LUMO energy levels and optical band gap by cyclic voltammetry and UV-VIS spectroscopy; (iii) investigation of solvatochromic behavior and spectral properties through UV-VIS spectroscopy in different solvents as well as in solid films; (iv) a photoisomerization study in nonpolar ($CHCl_3$) and polar aprotic (DMF) solvents by UV-irradiation at $\lambda = 365$ nm, supported by TD-DFT quantum chemical calculations as *trans (E)* and *cis (Z)* isomers.

2. Experimental

2.1. Used Materials

The 3-aminobenzyl alcohol (99%), 2-amino-5-nitrobenzonitrile (95%), 2.4-dinitroaniline (98%) and 4-bromo-2-methylaniline (97%) were purchased from Sigma Aldrich. The solvents, hydrochloric acid, sodium nitrite, sodium carbonate and urea were supplied from local supplier Valerus Ltd. For the spectral investigation all solvents were spectroscopy grade purity.

2.2. General Methodology for Synthesis of 4-Aminoazobenzenes

The starting substituted anilines (diazo components) were dissolved in 9 mL HCl_{conc} and 20 mL H_2O was added. The solution was then cooled to $T = 0$ °C in a salt/ice bath with stirring. Sodium nitrite (0.88 g, 11 mmole) in water (12 mL) was gradually added to this solution over 15 min period at $T = 0–5$ °C with stirring. The mixture was stirred for an additional 45 min to 1 h while maintaining at temperature of 0–5 °C. The excess of nitrous acid was destroyed by adding urea, and the solution was filtered. The resulting clear diazonium salt was used immediately in the azo-coupling reaction. The 3-aminobenzyl alcohol (azo component) was dissolved in 12 mL acetic acid and cooled to 0–5 °C in a salt/ice bath. The cold diazonium salt solution was added to this cooled solution over 20 min with vigorous stirring in a drop wise manner, while maintaining the pH 4–6 by addition of saturated sodium carbonate solution. The mixture was further stirred for 1 h at 0–5 °C and resulting solid was filtered, washed with cold water, dried, and recrystallized two times in ethanol. TLC $CHCl_3$:CH_3COOH 9:1. The reactions for preparation of azo dyes are presented on the Scheme 1.

2.2.1. Preparation of (E)-2-((4-Amino-2-(Hydroxymethyl)Phenyl)Diazenyl)-5-Nitrobenzonitrile, Azo-1

The Azo-1 was synthesized from 2-amino-5-nitrobenzonitrile 12.26 mmole (2 g) and 3-aminobenzyl alcohol 12.26 mmole (1.51 g), yield 43%, m.p. 157–160 °C. ATR-FTIR cm^{-1}: ν-OH 3404, ν^{as} -NH_2 3329, ν^{s} -NH_2 3232, ν -CH_2 2980, 2930, ν -C≡N 2229, δ -NH_2 1642, ν -NO_2 1494, ν -N═N- 1403. ^{1}H NMR (DMSO-d_6) ppm: 6.9–8.5 (m, 6H), 5.1 (s, 2H, —NH_2), 4.5 (s, 1H, —OH), 1.9 (s, 2H, —CH_2). Elemental analysis calculated for $C_{14}H_{11}N_5O_3$: C, 56.56; H, 3.73; N, 23.56; O, 16.15, Found: C, 55.98; H, 3.46; N, 24.06; O, 16.85.

2.2.2. Preparation of (E)-(5-Amino-2-((2.4-Dinitrophenyl)Diazenyl) Phenyl)Methanol, Azo-2

The Azo-2 was synthesized from 2,4-dinitroaniline 10.93 mmole (2 g) and 3-aminobenzyl alcohol 10.93 mmole (1.35 g), yield 61%, m.p. 121–124 °C. ATR-FTIR cm^{-1}: ν -OH 3453, ν^{as} -NH_2 3404, ν^{s} -NH_2 3330, ν -CH_2 2945, 2865, δ -NH_2 1628, ν -NO_2 (doublet) 1521, 1412, ν -N═N- 1388. ^{1}H NMR (DMSO-d_6) ppm: 6.9–8.5 (m, 6H), 5.4 (s, 3H, —NH_2, —OH), 2.8 (s, 2H, —CH_2). Elemental analysis calculated for $C_{13}H_{11}N_5O_5$: C, 49.22; H, 3.49; N, 22.07; O, 25.21, Found: C, 48.81; H, 3.32; N, 22.20; O, 25.44.

2.2.3. Preparation of (E)-(5-Amino-2-((4-Bromo-2-Methylphenyl) Diazenyl)Phenyl)Methanol, Azo-3

The Azo-3 was synthesized from 4-bromo-2-methylaniline 10.75 mmole (2 g) and 3-aminobenzyl alcohol 10.75 mmole (1.33 g), yield 41%, m.p. 142–146 °C. ATR-FTIR cm^{-1}: ν -OH 3404, ν^{as} -NH_2 3311, ν^{s} -NH_2 3175, ν -CH_2 and CH_3 2981, 2930, 2867, δ -NH_2 1613, ν -N═N- 1399. ^{1}H NMR (DMSO-d_6), ppm: 6.5–7.8 (m, 6H), 5.2 (s, 2H, —NH_2), 4.8 (s, 1H, —OH), 1.9 (s, 2H, —CH_2), 1.1 (s, 3H, —CH_3). Elemental analysis calculated for $C_{14}H_{14}BrN_3O$: C, 52.52; H, 4.41; Br, 24.96; N, 13.12; O, 5.00, Found: C, 53.57; H, 4.26; N, 13.45; O, 5.11.

2.3. Quantum Chemical Calculations

The optimization of molecular geometry and electronic structure of studied molecules were performed by GAUSSIAN 09W software package using density-functional theory DFT/B3LYP functional combined with the standard 6-31 + G(d,p) basis set both in vacuo and solvation in $CHCl_3$ [17]. The interactions between the molecule and the solvent were evaluated at the same basis set by polarizable continuum model (PCM) using the integral equation formalism variant (IEFPCM). The Natural Bonding Orbital (NBO) and charges distribution were computed

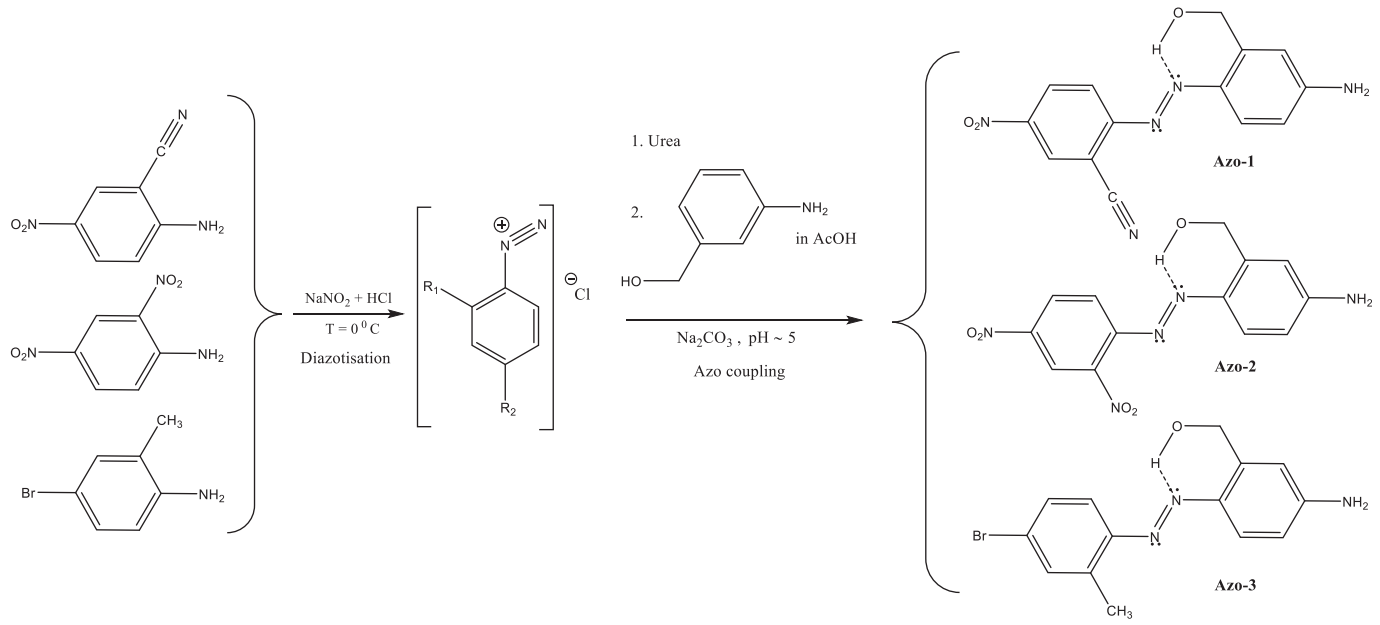

Scheme 1. Synthetic pathway of the 4-aminoazobenzene dyes (Azo-1, Azo-2 and Azo-3).

after optimization of geometry at the same basis set using $CHCl_3$ solvent. The frequency analysis was made at the same level of theory to characterize the stationary points on the potential surface and to obtain thermodynamic parameters such as absolute enthalpy (H) and Gibbs free energy (G) at 298 K. The precomputed vibrational scaling factor 0.964 was used according to the CCCBDB (Computational Chemistry Comparison and Benchmark Data Base) of National Institute of Standards and Technology, U.S. Department of Commerce [18]. The TD-DFT calculations were performed after optimization of geometry in *trans (E)* and *cis (Z)* azo dyes at the same basis set using $CHCl_3$ and DMF solvents.

2.4. Preparation of Thin Films

The thin films of Azo-1, Azo-2 and Azo-3 were prepared on quartz substrates by spin coating (speed 1500 rpm) of starting DMF solutions with concentration 5×10^{-6} mol L^{-1}, containing 2% (w/w) poly(methyl methacrylate) (PMMA) matrix. After coating, the films were subjected to the thermal annealing for 1 h at temperature 50 °C for solvent removal.

2.5. Photoisomerization Experiment

The photoisomerization of the azo dyes was performed in $CHCl_3$ and DMF solutions at room temperature (concentration 3.7×10^{-6} mol L^{-1}) by 4 W UVL-21 Compact UV lamp $\lambda = 365$ nm. The UV-VIS spectra were collected per 2 min from 0 to 20 min. Before investigation the samples were stored in dark overnight at room temperature.

2.6. Spectral Measurements

ATR-FTIR spectra of the compounds were recorded on a Bruker Tensor 27 FTIR spectrophotometer in the range 4400–600 cm^{-1} with resolution 2 cm^{-1} at room temperature. The external reflection diamond crystal has been used and the samples were scanned 128 times. The UV-VIS spectra have been done on the Cary 5E-UV-VIS-NIR. The first derivative spectra were performed by Savitzky–Golay algorithm with smoothing polynomial factor 10 and width of the peaks 7. The calibration curves of the dyes were plotted by several points of absorption measurements in different concentrations and molar extinction coefficients (ε_{max}) in $CHCl_3$, EtOH and DMF were calculated. The NMR spectra were collected on Spinsolve benchtop NMR spectrometer with frequency 43 MHz and resolution <0.7 Hz.

2.7. Cyclic Voltammetry Measurement

The voltammograms (CV) were recorded on a Metrohm 797 VA trace analyzer and a 797 VA stand. The Ag/AgCl, (3 mol L^{-1}) KCl electrode was used as the reference electrode, the hanging mercury drop electrode as the working electrode, and a platinum wire as the auxiliary electrode. All the voltammetric experiments were conducted in a high purity nitrogen atmosphere at room temperature (25 ± 1 °C). A 0.1 mol L^{-1} sodium acetate-acetic buffer (pH 5.5 ± 0.1) solution was used as a supporting electrolyte. The stock solutions (50 μM L^{-1}) of Azo-1, Azo-2 and Azo-3 were prepared by dissolution of the compounds in $CHCl_3$. Procedure: A 10 mL volume of sodium acetate-acetic buffer and 200 μl of Azo-1, Azo-2 and Azo-3 stock solutions (50 μM L^{-1}) were pipetted in the electrochemical cell. Oxygen was removed by bubbling pure nitrogen through the solution for 10 min. The voltamograms were registered at the following parameters: working electrode: HMDE with a drop size of ≈0.15 mm^2, Voltage step 5 mV, Sweep rate 0.100 mV s^{-1}. Adsorption was carried at −1.2 V for 60 s with continuous stirring at speed of 2000 rpm. The stirrer was stopped and the solution was allowed to rest for 10 s, then the voltammograms were recorded over reduction potential range from +0.020 to −1.2 V [19,20].

3. Results and Discussion

3.1. Background of Interpretation of the Results

Three 4-aminoazobenzene dyes (Azo-1, Azo-2 and Azo-3, see Scheme 1) were synthesized incorporating —CH_2OH group connected via intramolecular hydrogen bond to the —N═N— group in order to investigate their photochromic behavior. Positions 2′- and 4′- in the phenyl ring were selected for introduction of electron withdrawing (EW) or electron donating (ED) substituents to obtain unsymmetrical electron ("push-pull") distribution on the molecular backbone. In Azo-1 a —C≡N group was introduced as an EW at 2′-position and a —NO_2 group as a second EW at 4′-position. The Azo-2 was designed with two —NO_2 groups as EW at 2′- and 4′- positions. Finally, Azo-3 was synthesized with two ED groups: —CH_3 (+I effect) at 2′-position and —Br (—I and +M effects) at 4′-position. The optimized molecular geometry

of the *trans (E)* and *cis (Z)* isomers were computed at DFT/B3LYP 6-31 + G(d,p) level of theory in vacuo and solvation using IEFPCM in $CHCl_3$ and DMF solvent. The NBO analysis was performed to evaluation the charge transfers (CT) and resonance energy on molecular backbone of *trans (E)* and *cis (Z)* azo dyes. The energy of frontier highest occupied molecular orbital (HOMO), lowest unoccupied molecular orbital (LUMO) and E_g (energy band gap) were computed and experimentally estimated by cyclic voltammetry and UV-VIS spectroscopy. The solvatochromic behavior was investigated in three different solvents $CHCl_3$ (nonpolar), EtOH (polar protic) and DMF (polar aprotic) to characterize the influence of the polarity on electron transitions energy. The photoisomerization of the azo chromophores was performed in $CHCl_3$ and DMF at room temperature with λ = 365 nm UV-irradiation and light intensity 4 W at equal concentrations and irradiation time. The electron transitions spectra and excitation energies of *trans (E)* and *cis (Z)* azo dyes were computed by TD-DFT using IEFPCM in $CHCl_3$ and DMF solvent in order to understand the electron transitions and molecular contributions, which are referred to the experimental results.

3.2. Quantum Chemical Calculations and Solvatochromism

The molecular backbone of *trans (E)* isomers has a trigonal planar geometry, whereas the —CH_2OH (hydroxymethyl) group is out of the plane and angles between tetrahedral sp^3 hybridized carbon, oxygen and hydrogens atoms are approximately 106°. This leads to a formation of intramolecular six-membered ring hydrogen bond with nonbonding electron pairs of the azo nitrogens. The optimized *cis (Z)* isomers are nonplanar, where the two phenyl rings are twisted in respect to the C—N═N—C with dihedral angles: −14.32° (Azo-1), −17.86° (Azo-2) and −11.49° (Azo-3). The calculated bond parameters and X,Y,Z coordinates of the azo chromophores as *trans (E)* and *cis (Z)* isomers are given in Supplementary information Tables S.1, S.2, S.3, S.4, S.5 and S.6. On Figs. 3 and 4 the molecular geometry optimized at DFT/B3LYP 6-31 + G(d,p) level of theory using IEFPCM in $CHCl_3$ solvent of the *trans (E)* and *cis (Z)* Azo-1, Azo-2 and Azo-3 are presented.

The lengths of the intramolecular hydrogen bonds in *trans (E)* isomers are shortened with the decrease of the conjugation and "push-pull" character of substituents in the phenyl rings: 2.212 Å (Azo-1) > 2.175 Å (Azo-2) > 2.128 Å (Azo-3). This means that nonbonding electron pair of Azo-3 is weakly conjugated with the phenyl ring and has a great capacity to donate electrons for hydrogen bonding. The EW —C≡N and —NO_2 groups of Azo-1 and Azo-2 involve the nonbonding azo nitrogens electron pairs in n-π conjugation. For this reason, EW substituents in *ortho-* and *para-* positions decrease the electron density and lead to weaker intramolecular hydrogen bonds. The *cis (Z)* azo dyes are in twisted conformation, where the lengths of the hydrogen bonds are bigger than in the *trans (E)* isomers. The -NH_2 hydrogens are out of the plane in the phenyl rings and n-π, π-π conjugation of azo groups with aromatic systems are decreased. Table 1 presents the calculated total electronic energy *E (RB3LYP)* and dipole moment μ of the azo chromophores in *trans (E)* and *cis (Z)* isomers.

The $\Delta E_{trans \rightarrow cis}$ and $\Delta\mu_{trans \rightarrow cis}$ were defined as difference between final state (f) *cis (Z)* isomers (products of the photochemical reaction) and initial state (i) *trans (E)* (reactants). For Azo-1 and Azo-2 the $\Delta E_{trans \rightarrow cis}$ have similar values, which indicate unfavorable energetic state (higher energy) in *cis (Z)* isomers. The change of the energy of Azo-3 is smaller compared to the Azo-1 and Azo-2. The reasons are significant decrease of the conjugation on the molecular backbone and orbital repulsions between substituents and phenyl rings. The molecular dipole moment is a vector sum of bond dipole moments and mainly depends on molecular geometry (relative orientation of the bonds). Less dipole moments in *cis (Z)* compared to *trans (E)* isomers means that the bonds polarity are decreased and the direction of vector dipoles of the bonds are opposite and canceled each other. The $\Delta\mu_{trans \rightarrow cis}$ values of Azo-1 and Azo-2 show significant decrease compared to the Azo-3 due to the polarization of the molecular backbone by EW and ED groups. The calculated thermodynamic parameters absolute enthalpy H_{298} (sum of electronic and thermal enthalpies) and free Gibbs energy G_{298} (sum of electronic and thermal free Gibbs energies) related to the $\Delta H_{trans \rightarrow cis}$, $\Delta G_{trans \rightarrow cis}$ and $\Delta S_{trans \rightarrow cis}$ are presented in Table 2.

The parameters of H_{298} and G_{298} between *cis (Z)* and *trans (E)* isomers are given by $\Delta H_{trans \rightarrow cis}$ and $\Delta G_{trans \rightarrow cis}$, where the differences in energies of Azo-1 and Azo-2 are higher than Azo-3. The $\Delta H_{trans \rightarrow cis} > 0$ and $\Delta G_{trans \rightarrow cis} > 0$ show that $E \rightarrow Z$ isomerisation is

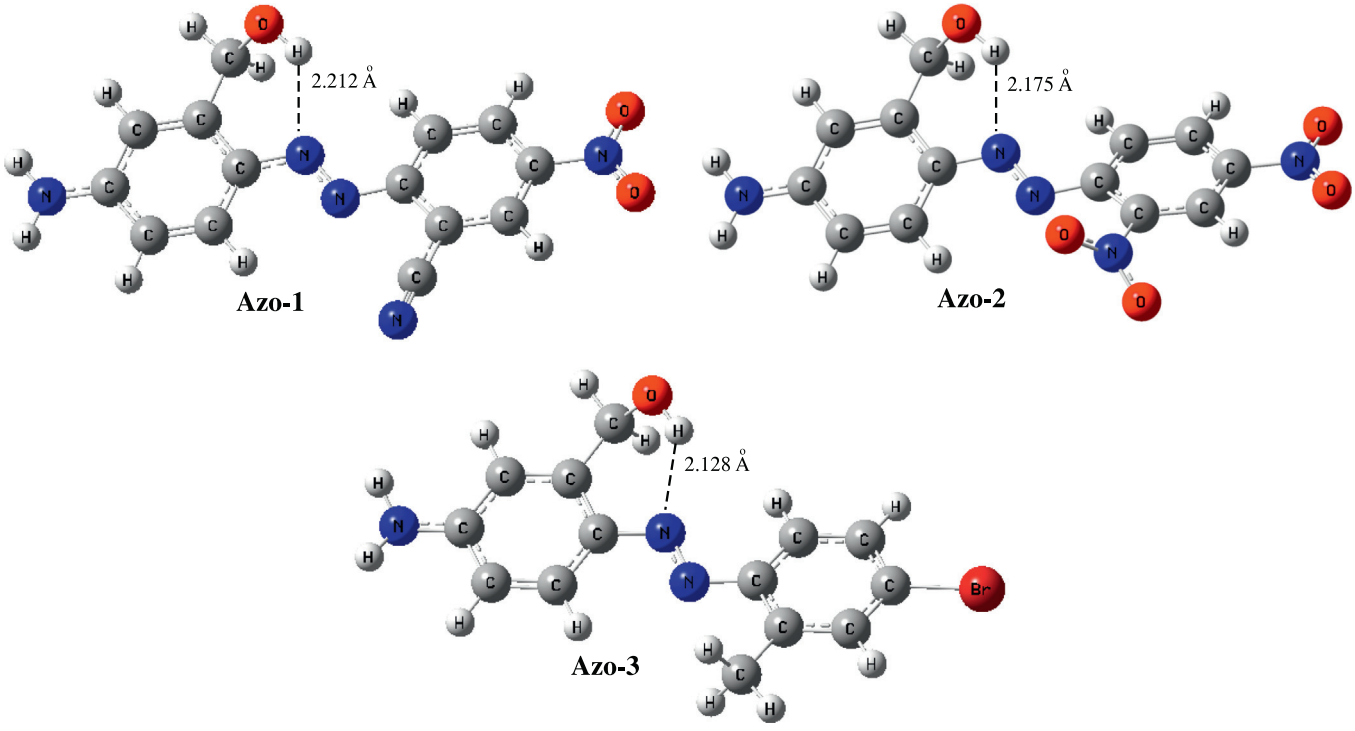

Fig. 3. Molecular geometry and intramolecular H-bond of trans (E) Azo-1, Azo-2 and Azo-3 isomers optimized at DFT/B3LYP 6-31 + G(d,p) level of theory using IEFPCM in $CHCl_3$ solvent.

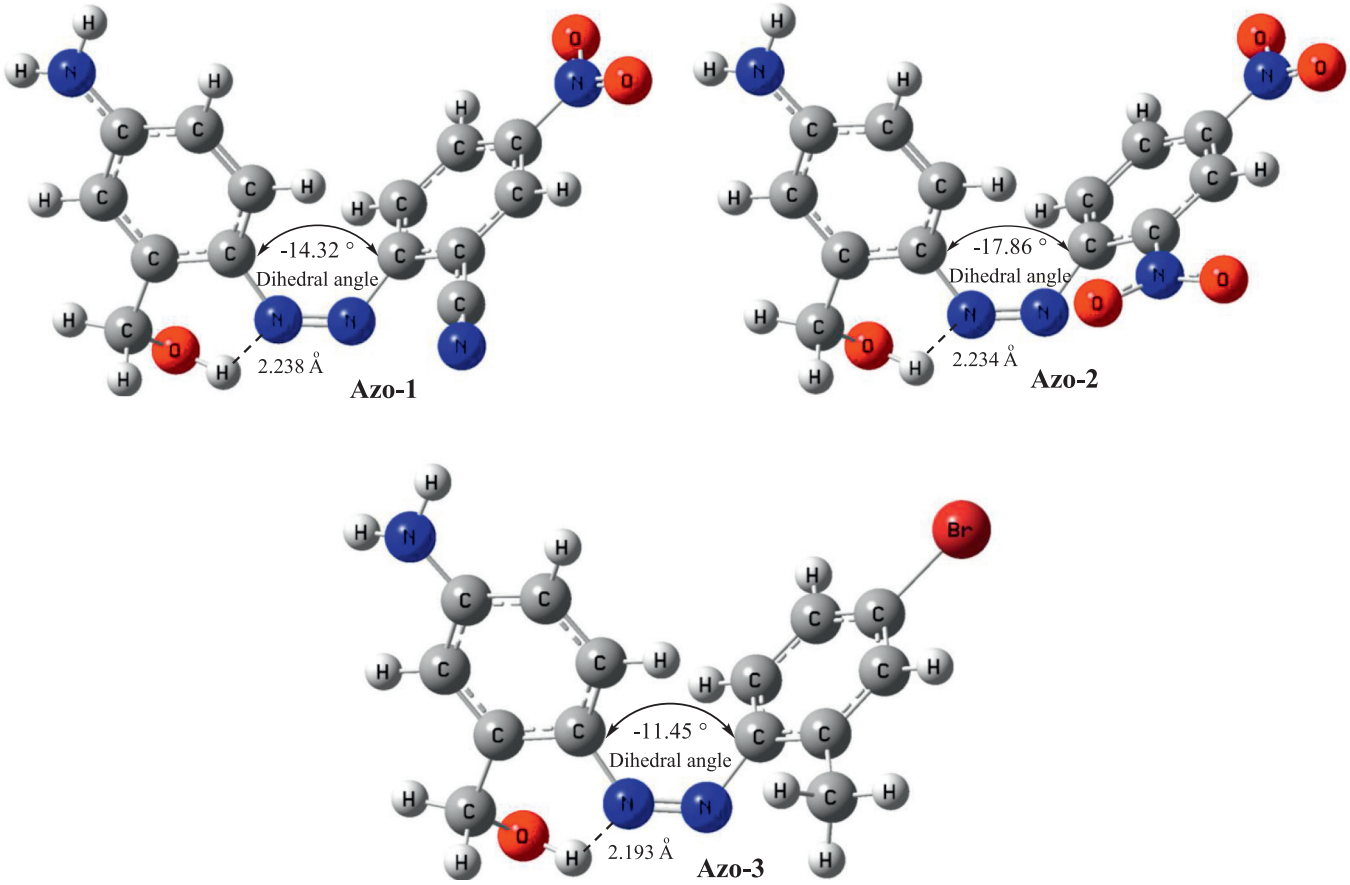

Fig. 4. Molecular geometry and intramolecular H-bond of cis (Z) Azo-1, Azo-2 and Azo-3 isomers optimized at DFT/B3LYP 6-31 + G(d,p) level of theory using IEFPCM in $CHCl_3$ solvent.

reversible photochemical reaction and does not occur spontaneous without UV irradiation to a less stable *cis (Z)* isomer. The $\Delta S_{trans \rightarrow cis}$ of Azo-1 increases, while for Azo-2 and Azo-3 decrease. The $\Delta S_{trans \rightarrow cis}$ is related to the order of the macroscopic system and probability of photoisomerization reactions to *cis (Z)* isomers. For Azo-1 the change of entropy has a positive value because of higher $\Delta H_{trans \rightarrow cis}$ and $\Delta G_{trans \rightarrow cis}$. This indicates that Azo-1 and Azo-2 are more stable in *trans (E)* isomers, while for Azo-3 the photoisomerization to *cis (Z)* isomer is favored by the kinetic factor. The computed and experimental values of vibrational bands of the chromophores are given in Supplementary information Tables S.7, S.8 and S.9 and Figs. S.1, S.2 and S.3 [21]. The frequencies of the IR bands of ν —OH, ν —NH_2 for *cis (Z)* isomers are higher compared to the *trans (E)* isomers. The calculated bands of ν —N═N— for *trans (E)* isomers are in a good agreement with the experimental results, whereas for the *cis (Z)* isomers are not registered (Azo-1 and Azo-2) due to the symmetric vibrations, where $(\frac{d\mu}{dr})r_0 = 0$. The computed HOMO and LUMO frontier orbitals and surface electron distributions of the azo chromophores are presented in Supplementary information Figs. S.4, S.5 and S.6.

The natural charges of atoms in functional groups provide information about molecular polarizability, electronic structure and charge affects on dipole moment. The natural bond orbitals (NBO) analysis and second order Fock matrix are carried out by considering all possible interactions between (donor) Lewis NBOs and (acceptor) non Lewis NBOs. The intramolecular charge transfers (CT) or conjugations on molecular backbone are the main features of photochromic properties of the molecules. For each donor NBO (i) and acceptor NBO (j), the resonance stabilization energy associated with i → j delocalization can be evaluated as (Eq. (1)),

$$E(2) = \Delta E_{ij} = q_i \frac{F(i,j)^2}{\varepsilon_j - \varepsilon_i} \quad (1)$$

where q_i is the donor orbital occupancy, ε_j and ε_i are diagonal elements and $F_{(i,j)}$ is the off diagonal NBO Fock matrix element [21,22,23]. The natural charges and NBOs analysis of azo dyes are presented on Fig. 5 and Table 3. Significant changes of charges and resonance energy of the azo nitrogens (—N═N—) acceptor and lone pair (LP) -NH_2 group

Table 1
Theoretical calculations of the total electronic energy E (RB3LYP) and dipole moment μ of trans (E) and cis (Z) isomers of the azo dyes by DFT/B3LYP 6-31 + G(d,p) level of theory using IEFPCM in $CHCl_3$ solvent.

Compounds	E (RB3LYP) [kcal mol^{-1}]		μ [D]		$\Delta E_{trans \rightarrow cis}$ [kcal mol^{-1}]*	$\Delta\mu_{trans \rightarrow cis}$ [D]**
	Trans	Cis	Trans	Cis		
Azo-1	−652,277.1922	−652,250.2093	14.355	9.139	26.9829	−5.216
Azo-2	−722,718.7037	−722,695.1094	14.616	8.975	23.5944	−5.641
Azo-3	−2,104,141.62	−2,104,135.533	7.341	5.594	6.08685	−1.747

* $\Delta E = E_{tcis} - E_{itrans}$.
** $\Delta\mu = \mu_{tcis} - \mu_{trans}$.

Table 2
Theoretical calculations of the thermodynamic parameters of *trans (E) and cis (Z)* isomers of the azo dyes by DFT/B3LYP 6-31 + G(d,p) level of theory using IEFPCM in $CHCl_3$ solvent.

Compounds	H_{298} [kcal mol^{-1}]		G_{298} [kcal mol^{-1}]		$\Delta H_{trans \rightarrow cis}$ [kcal mol^{-1}]*	$\Delta G_{trans \rightarrow cis}$ [kcal mol^{-1}]**	$\Delta S_{trans \rightarrow cis}$ [cal K^{-1} mol^{-1}]***
	Trans	Cis	Trans	Cis			
Azo-1	−652,113.3926	−652,086.6707	−652,157.1828	−652,130.9842	26.7219	26.1985	1.7563
Azo-2	−722,552.2235	−722,526.7732	−722,597.851	−722,572.2002	25.4503	25.6507	−0.6724
Azo-3	−2,103,967.922	−2,103,946.839	−2,104,009.826	−2,103,988.652	21.0831	21.1741	−0.3053

* $\Delta H = H_{fcis} - H_{itrans}$.
** $\Delta G = G_{fcis} - G_{itrans}$.
*** $\Delta S = \frac{\Delta H - \Delta G}{T}$.

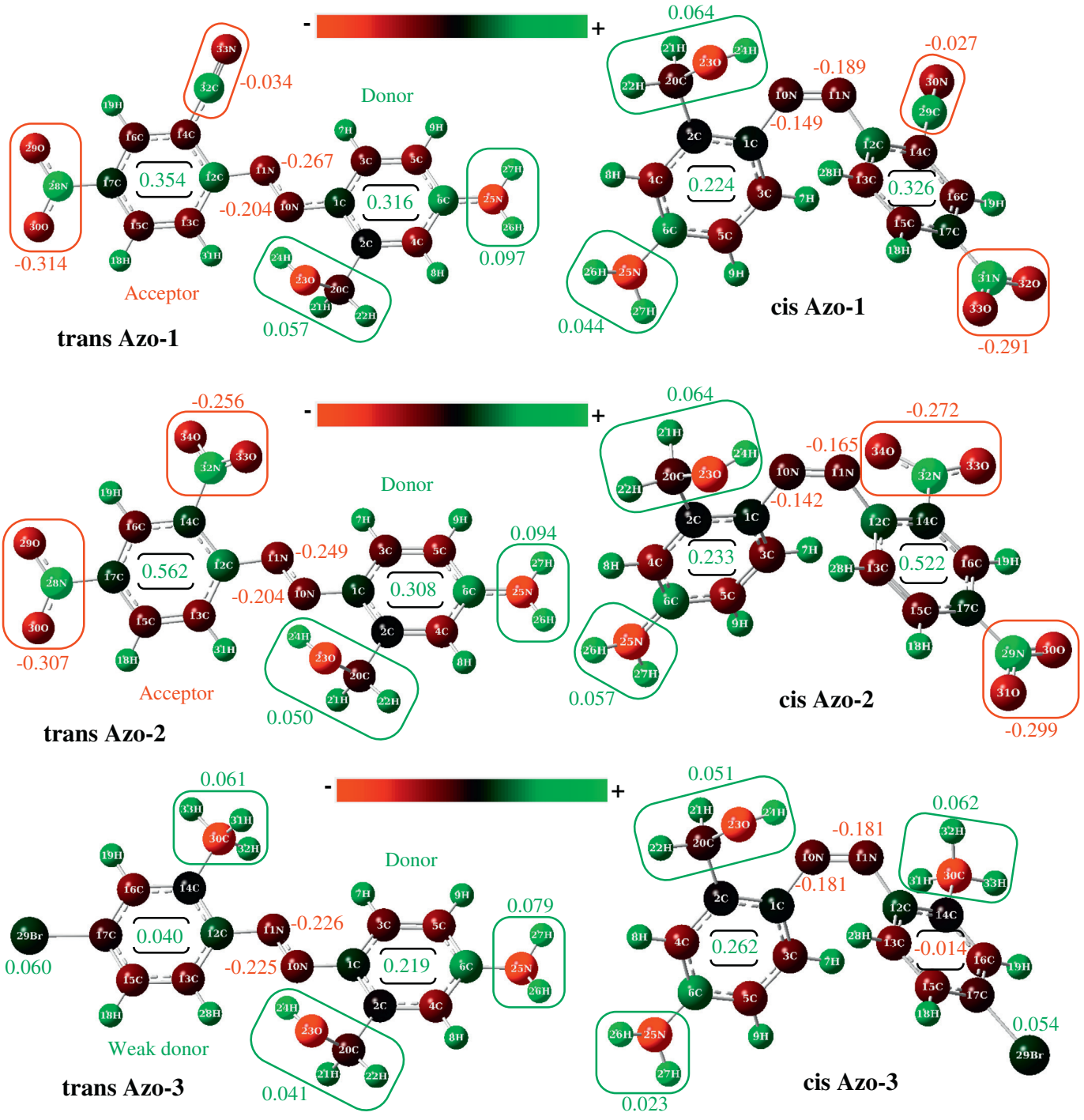

Fig. 5. NBO charges of *trans (E)* and *cis (Z)* azo dyes isomers calculated at DFT/B3LYP 6-31 + G(d,p) level of theory using IEFPCM in $CHCl_3$ solvent. Charges transfer on molecular backbones are presented as summing the atoms charges in functional groups and phenyl rings. The charges distribution are marked as donor and acceptor parts of the dyes connected via azo bridge.

Table 3
Second order perturbation theory analysis of Fock matrix in NBO basis of azo dyes calculated by DFT/B3LYP 6-31 + G(d,p) level of theory using IEFPCM in $CHCl_3$ solvent.

Compounds	Donor NBO (i)	Acceptor NBO (j)	E(2) [kcal mol^{-1}]	E(j)-E(i) [a.u]	F(i,j) [a.u]
trans (E) Azo-1	LP(1) N25	π* C5–C6	48.74	0.28	0.107
	LP(2) O23	σ* C2–C20	6.92	0.70	0.063
	π C1–C3	π* N10–N11	27.91	0.21	0.070
	π N10–N11	π* C12–C13	13.39	0.38	0.068
	LP(1) N10	LP*(1) H 24	5.15	0.61	0.056
	LP(1) N11	LP*(1) H 24	0.20	0.60	0.011
	LP(1) N10	σ* C1–C3	8.92	0.95	0.083
	LP(1) N11	σ* C12–C13	8.61	0.94	0.081
	π C14–C16	π* C32–N33	19.08	0.37	0.081
	π C15–C17	π* N28–O30	31.62	0.13	0.061
	σ C15–C17	σ* N28–O29	2.50	1.13	0.048
cis (Z) Azo-1	LP(1) N25	π* C4–C6	34.32	0.30	0.096
	LP(2) O23	σ* C2–C20	8.26	0.71	0.068
	π C1–C2	π*N10–N11	22.27	0.22	0.065
	π N10–N11	π* C12–C13	3.47	0.39	0.036
	LP(1) N10	LP*(1) H 24	4.36	0.60	0.051
	LP(1) N10	σ* C1–C3	7.54	0.94	0.076
	LP(1) N11	σ* C12–C13	3.52	0.92	0.052
	π C14–C16	π* C29–N30	12.65	0.37	0.066
	π C15–C17	π* N31–O32	32.56	0.13	0.063
	σ C15–C17	σ* N31–O32	2.33	1.14	0.046
trans (E) Azo-2	LP(1) N25	π* C5–C6	48.43	0.28	0.107
	LP(2) O23	σ* C2–C20	6.99	0.70	0.063
	π C1–C3	π* N10–N11	27.15	0.21	0.06
	π N10–N11	π* C12–C13	11.39	0.38	0.063
	LP(1) N10	LP*(1) H24	6.10	0.61	0.061
	LP(1) N11	LP*(1) H24	0.23	0.61	0.012
	LP(1) N10	σ* C1–C3	8.84	0.95	0.083
	LP(1) N11	σ* C12–C13	7.23	0.93	0.074
	π C14–C16	π* N32–O33	20.72	0.15	0.054
	π C14–C16	σ* N32–O34	1.14	0.68	0.027
	π C15–C17	π* N28–O29	34.68	0.13	0.065
	π C16–C17	σ* N28–O29	2.45	1.14	0.047
cis (Z) Azo-2	LP(1) N25	π* C5–C6 or π* C4–C6	–	–	–
	LP(2) O23	σ* C2–C20	8.37	0.71	0.069
	σ C1–C2	σ* N10–N11	2.78	1.26	0.053
	π N10–N11	π* C12–C13	3.03	0.38	0.034
	LP(1) N10	σ* O23–H24	2.60	0.89	0.044
	LP(1) N10	σ* C1–C3	7.70	0.94	0.077
	LP(1) N11	π* C12–C14	18.79	0.37	0.081
	π C12–C14	π* N32–O34	26.43	0.15	0.059
	π C12–C14	σ* N32–O33	2.12	1.15	0.044
	π C16–C17	π* N29–O30	28.30	0.14	0.061
	σ C16–C17	σ* N29–O31	2.31	1.15	0.046
trans (E) Azo-3	LP(1) N25	LP*(1) C6	69.37	0.17	0.120
	LP(2) O23	σ* C2–C20	6.80	0.71	0.062
	LP(2) Br29	σ* C15–C17	3.04	0.85	0.045
	LP(1) N10	σ* O23–H24	4.71	0.90	0.059
	LP(1) N10	σ* C1–C3	8.40	0.97	0.081
	LP(1) N11	σ* C12–C13	8.05	0.96	0.097
	σ C1–C3	σ* N10–N11	2.30	1.26	0.048
	π N10–N11	π* C12–C13	37.21	0.05	0.068
	π C15–C17	LP*(1) Br29	1.42	0.73	0.032
	σ C30–H31	π* C14–C16	3.52	0.52	0.042
	σ C30–H32	π* C14–C16	3.15	0.52	0.039
	σ C30–H33	σ* C12–C14	4.43	1.06	0.061
cis (Z) Azo-3	LP(1) N25	LP*(1) C6	67.66	0.17	0.119
	LP(2) O23	σ* C2–C20	8.14	0.71	0068
	LP(2) Br29	σ* C15–C17	3.04	0.85	0.045
	LP(1) N10	σ* O23–H24	3.13	0.88	0.048
	LP(1) N10	σ* C1–C3	7.67	0.94	0.077
	LP(1) N11	π* C12–C14	8.80	0.41	0.058
	σ C1–C2	σ* N10–N11	2.88	1.26	0.054
	π N10–N11	π* C12–C14	3.08	0.41	0.035
	π C16–C17	LP*(1) Br29	1.49	0.73	0.032
	σ C30–H31	π* C12–C14	3.42	0.52	0.042
	σ C30–H32	π* C12–C14	2.45	0.52	0.035
	σ C30–H33	σ* C12–C14	4.36	1.06	0.061

donor from *trans (E)* to *cis (Z)* conversion for all azo dyes are observed. The changes are decreased in order: (—N═N—) Azo-2 > Azo-1 > Azo-3 and (—NH_2) Azo-3 > Azo-1 > Azo-2. This means that conjugation and CT in *cis (Z)* isomers are decreased compared to the *trans (E)* isomers. The stabilization energy E(2) indicates the intensive interaction between electron donors and electron acceptors and greater the extent of conjugation of the whole system in *trans (E)* isomers. This indicates that Azo-1 and Azo-2 are more stable in *trans (E)* isomers because of the energy of resonance stabilization and effectively π-π conjugation. The relative higher stability of Azo-3 in *cis (Z)* could be explained by the lower resonance energy and π-π conjugation. It should be remarked that azo LP(1) N10 and hydroxymethyl LP*(1) H 24 (—OH) have E(2) ~ 5–6 kcal mol^{-1}, while the azo LP(1) N11 and hydroxymethyl LP*(1) H 24 (—OH) this energy is approximately zero. This fact demonstrates that there are an intramolecular six-membered hydrogen bonds in azo dyes.

The investigation of the electronic spectral features of the azo compounds is important in order to estimate the electron transitions energy, optical band gap and HOMO-LUMO energy levels of frontier orbitals. These parameters determine the possible application of the molecules for optoelectronic devices such as optical photoswitches, optical storage information and solar cells. The energy of HOMO frontier orbitals and the optical band gap are determined by cyclic voltammetry (Supplementary information, Fig. S.7) and UV-VIS spectroscopy by the absorption edge. In the cyclic voltammetry ferrocence is used as a known reference value of −4.4 eV to calculate the energy of the HOMO by E_{ox} *onset* (Eq. (2)):

$$\mathrm{HOMO} = -\mathrm{e}\,[E_{Ox}(\mathrm{onset}) + 4.4] \tag{2}$$

where, E_{ox} *onset* represents the experimentally determined value of the oxidation potential.

In organic molecules, the energy levels of the electronic states correspond to the energy carried by UV or VIS radiation. At resonance, the molecules can absorb quantified energy transported by the electromagnetic radiation, and promote an electron from the low energy molecular orbital to the higher one [24,25]. These transitions can be measured using a UV-VIS spectrophotometer, where E_g corresponds to the energy of the long wavelength edge of the excitation absorption band [24,25,26]. The longest absorption wavelength λ_{onset} is used to calculate the optical gap energy, E_g, according to the Eq. (3) [26]:

$$\mathrm{E}_g = h.\nu = \frac{h.c}{\lambda} = \frac{1242}{\lambda} \tag{3}$$

The LUMO energy was calculated according to Eq. (4):

$$\mathrm{LUMO} = \mathrm{HOMO} + \mathrm{Eg} \tag{4}$$

It is possible to define the optical band gap as a difference between the HOMO and LUMO of a species created by photoexcitation of electrons. From the other hand, the electrochemical band gap is a difference, between reduction and oxidation potentials of the species. Electrochemical reduction requires higher energy than LUMO and also for oxidation the energy should be lower than HOMO. These extra energy requirements for red-ox produce a difference between the electrochemical band gap and optical band gap. The reason could be the exciton binding energy, if electrochemical band gap energy is less than optical band gap, other factors such as solvation, dipole-dipole interactions and electrode surface phenomena might play a role [27]. The schematic representation of the differences between optical and electrochemical band gap is illustrated on Fig. 6.

Fig. 7 and Table 4 present the computed and experimentally estimated energy levels of HOMO and LUMO frontier orbitals and E_g of azo dyes.

The computed and experimental energy levels are quite different, especially for HOMO levels. This could be attributed to absence of direct electron transitions between HOMO and LUMO. The solvation of the molecules, dipole-dipole interactions and the surface properties of the electrode are the other influencing factors. The computed and experimental E_g for Azo-1 and Azo-2 are close, while for Azo-3 the difference is 0.9 eV.

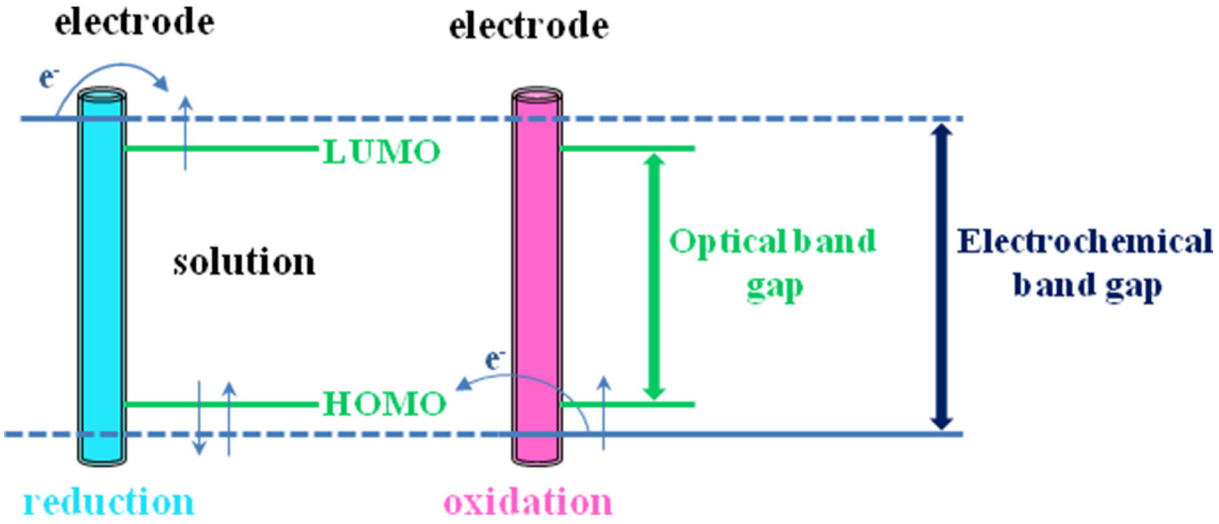

Fig. 6. Schematic illustration between optical and electrochemical band gap, adapted from S.N. Inamdar et al. [27].

The behavior of the dyes in solvents with different polarity corresponds to interactions between the azo dipoles and solvent molecules. The solvatochromic shifts in $CHCl_3$, EtOH and DMF of Azo-1, Azo-2 and Azo-3 (Fig. 8) were investigated and molar extinction coefficient (ε_{max}), oscillator strength (f) and transition dipole moment (μ^2) have been calculated form UV-VIS spectra (Table 5). Oscillator strength, f, was calculated by the following equation (Eq. (5)) [28,29]:

$$f = 4.319 \times 10^{-9} \int \varepsilon(\bar{\upsilon}) d\bar{\upsilon} \tag{5}$$

where, ε molar absorptive [L mol^{-1} cm^{-1}], $\bar{\upsilon}$ wavenumber [cm^{-1}]

Transition dipole moment, μ^2, was found from the equation (Eq. (6)) [28,29]:

$$\mu^2 = \frac{3e^2\,\hbar}{4\pi m_e \bar{\upsilon}} \times f \tag{6}$$

where, $\hbar$ is reduced Planck constant [eV·s]; m_e is mass of the electron [eV]; e is charge of the electron [esu].

The electron transition $\pi \rightarrow \pi^*$ ($S_0 \rightarrow S_2$) and $n \rightarrow \pi^*$ ($S_0 \rightarrow S_1$) bands of Azo-1 and Azo-2 are well separated due to the unsymmetrical electron distributions (push-pull) of EW groups, while in the spectra of Azo-3 they are overlapped in a broad peak because of properties of the ED groups. In nonpolar solvent $CHCl_3$ Azo-1 has absorption of $\pi \rightarrow \pi^*$ at $\lambda_{max} = 330$ nm and $n \rightarrow \pi^*$ at $\lambda_{max} = 462$ nm. Increasing the solvent polarity leads to a strong bathochromic shift in EtOH ($\pi \rightarrow \pi^*$ at $\lambda_{max} = 341$ nm and $n \rightarrow \pi^*$ at $\lambda_{max} = 512$ nm) and DMF ($\pi \rightarrow \pi^*$ at $\lambda_{max} = 360$ nm and $n \rightarrow \pi^*$ at $\lambda_{max} = 534$ nm). The UV-VIS spectrum of Azo-2 in $CHCl_3$ is quite interesting because of two separated bands appearing in the UV region for $\pi \rightarrow \pi^*$ $\lambda_{max1} = 329$ nm and $\lambda_{max2} = 378$ nm, while in the VIS region $n \rightarrow \pi^*$ is at $\lambda_{max} = 473$ nm. The existence of two bands in UV range are due to the competitive electron resonance distributions between azo π system and *ortho* nitro group related to the HOMO → LUMO + 1 transition (Supplementary information Table S.14 and S.16). The solvent polarity also causes strong solvatochromic shift to lower energy (red shift) in EtOH (for $\pi \rightarrow \pi^*$ $\lambda_{max1} = 336$ nm and $\lambda_{max2} = 386$ nm, for $n \rightarrow \pi^*$ $\lambda_{max} = 512$ nm) and DMF (for $\pi \rightarrow \pi^*$ $\lambda_{max1} = 346$ nm and $\lambda_{max2} = 397$ nm, for $n \rightarrow \pi^*$ $\lambda_{max} = 533$ nm). The overlapping $\pi \rightarrow \pi^*$ and $n \rightarrow \pi^*$ electron transition bands of Azo-3 exhibit solvatochromic behavior by shifting of the absorption maximum in $CHCl_3$ at $\lambda_{max} = 384$ nm, EtOH at $\lambda_{max} = 411$ nm and DMF at $\lambda_{max} = 420$ nm. All azo compounds have shown strong solvation by dipole interactions with the solvents, which leads to a decrease energy of the electron transitions. The electronic spectra of solid films of the azo

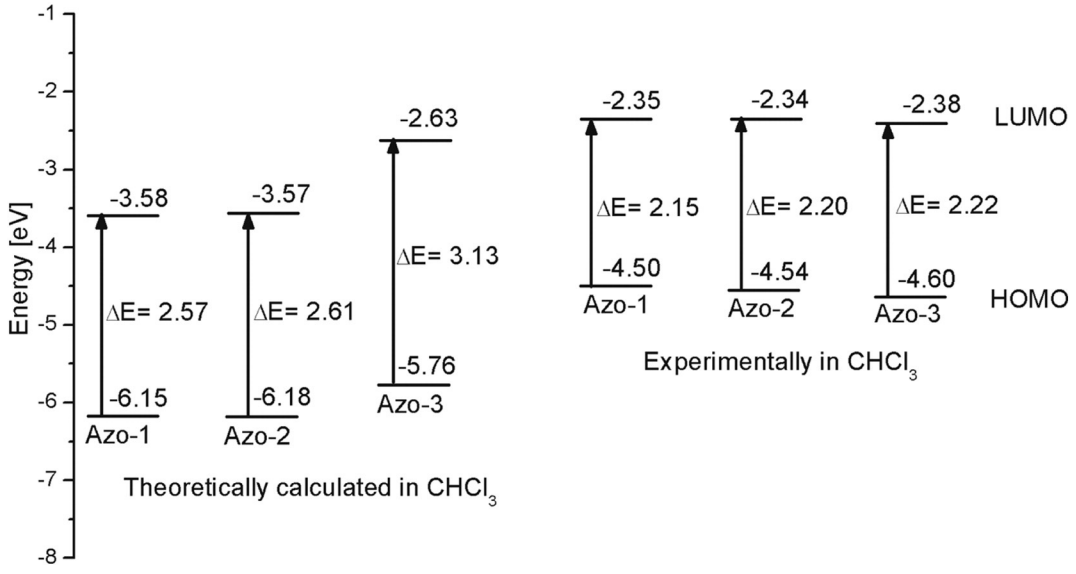

Fig. 7. Computed and experimentally estimated in $CHCl_3$ energy levels of HOMO and LUMO frontier orbitals of the azo dyes.

Table 4
Theoretically and experimentally estimated HOMO and LUMO energy levels of frontier orbitals of the *trans (E)* azo compounds in $CHCl_3$.

Compounds	Theoretically calculated [eV]			E_{ox} (onset) [V]	Absorption edge [nm]	Experimentally estimated [eV]		
	HOMO	LUMO	E_g			HOMO	LUMO	E_g
Azo-1	−6.15	−3.58	2.57	−0.10	577	−4.50	−2.35	2.15
Azo-2	−6.18	−3.57	2.61	−0.14	566	−4.54	−2.34	2.20
Azo-3	−5.76	−2.63	3.13	−0.20	562	−4.60	−2.38	2.22

chromophores in PMMA matrix have similar energy to the spectra in EtOH. This means that there are strong dipole-dipole interactions between the chromophores and matrix as well as the solid state intermolecular dipole interactions between the azo molecules.

It might be concluded that the oscillator strength *f* depends on the symmetry of frontier molecular orbitals, where the electron transitions are allowed, moreover the electron levels are affected by the solvents (Table 5). The *f* for $n \rightarrow \pi^*$ ($S_0 \rightarrow S_1$) transitions are increased by the solvents polarity, whereas for $\pi \rightarrow \pi^*$ ($S_0 \rightarrow S_2$) are decreased. The transition dipole moment μ^2 depends strongly on *f* and on the nature of the molecules. It can be seen that solvation in protic polar solvent EtOH has a stronger transition dipole moment, which may be due to the EtOH—Azo dyes hydrogen bonding.

3.3. Photoisomerization

The photoisomerization is an important characteristic of azo compounds and the energy of this conversion depends on the previously discussed parameters - solvatochromism, *f*, μ^2, E_g, and by energy and intensity of the UV light and time of irradiation. The experiments were conducted for the three azo dyes at identical concentrations and time of illumination in two solvents: $CHCl_3$ and DMF. The aim was to evaluate the influence of the solvents on the photochromic properties of the azo dyes in relation to the energy of the electron transitions and intramolecular hydrogen bonding. The degree of photoisomerization at the photostationary state, *R*, was evaluated according to the equation (Eq. (7)) [30]:

$$R = \frac{(A_0 - A_\infty)}{A_0} \times 100 \tag{7}$$

where A_0 is the initial absorbance and A_∞ is the absorbance at the photostationary state.

The absorbance bands of molar electron transitions are not narrow as atomic transitions. The reason for this is overlapping of the ground state energy, oscillation energy and rotational energy of molecules as well as the interaction of the dyes with the solvents. Derivative spectra enhance resolution of the overlapped bands since changes in the

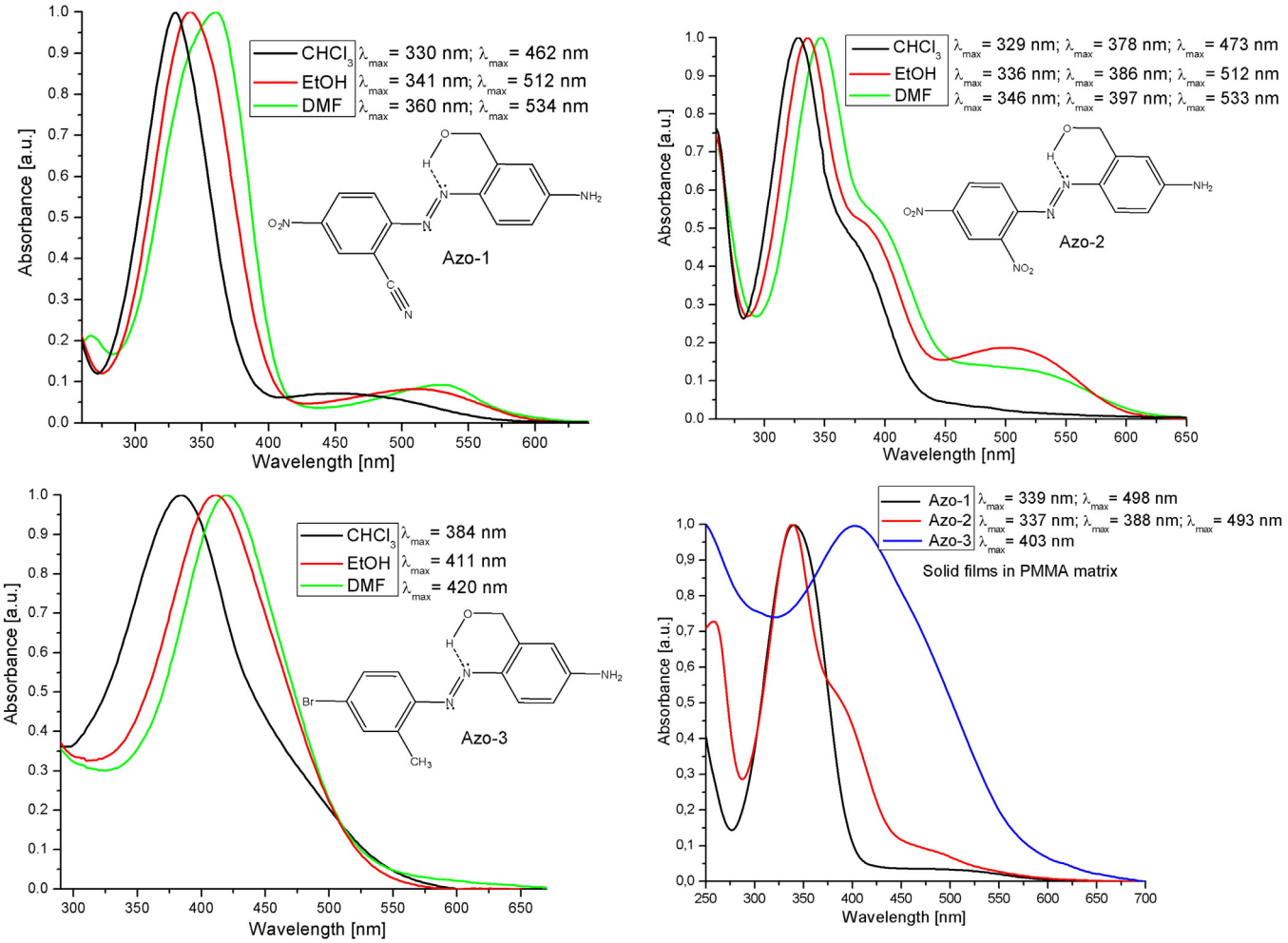

Fig. 8. Normalized UV-VIS spectra of the azo dyes in $CHCl_3$, EtOH, DMF solutions (conc. 5×10^{-6} mol L^{-1}) and solid films.

Table 5
Experimentally calculated solvatochromic shifts (Δλ), molar extinctions (ε_{max}), oscillator strength (f) and transition dipole moment (μ^2) of the azo chromophores in different polar solvents.

Compounds	λ_{max} [nm]			Δλ [nm]	ε_{max} [L mol^{-1} cm^{-1}]			*f*			μ^2 [D]		
	$CHCl_3$	EtOH	DMF		$CHCl_3$	EtOH	DMF	$CHCl_3$	EtOH	DMF	$CHCl_3$	EtOH	DMF
Azo-1	330	341	360	30	3.145×10^4	2.902×10^4	2.483×10^4	0.412	0.368	0.230	2.2	2.03	1.34
	462	512	534	72	7.0257×10^2	2.320×10^3	2.03×10^3	0.01	0.020	0.016	0.15	0.17	0.13
Azo-2	329	336	346	17	2.475×10^4	2.403×10^4	2.243×10^4	0.324	0.308	0.280	1.64	1.68	1.57
	378	386	397	19	1.126×10^4	1.355×10^4	1.205×10^4	0.129	0.114	0.131	1.99	0.71	0.85
	473	512	533	60	8.721×10^2	3.84×10^3	1.67×10^3	0.01	0.035	0.013	0.16	0.29	0.11
Azo-3	384	411	420	36	1.343×10^4	2.045×10^4	1.272×10^4	0.151	0.214	0.130	0.98	1.42	0.89

gradient are examined. First derivative (FD) emphasizes band widths, because the first derivative of most band shapes has maxima and minima near the half-height points of the bands. The spectrum is expressed as absorbance, *A*, as a function of wavelength, λ, where the zero and derivative spectra are [31]:

$A = f(\lambda)$ Zero order

$\frac{dA}{d\lambda} = f'(\lambda)$ First order

Figs. 9, 10 and 11 present the absorption and first derivative (FD) UV-VIS spectra of the photoisomerization of Azo-1, Azo-2 and Azo-3 in $CHCl_3$ and DMF for 20 min UV-irradiation with λ = 365 nm. Table 6 summarizes the calculated values of the photoisomerization degree in both solvents.

The UV-VIS spectra of Azo-1 in $CHCl_3$ (Fig. 9) with progress of the irradiation time the n → π* transitions decreased and reached zero absorbance with 20 min period. The π → π* transitions manifest only weak changes of the absorption band. This can be confirmed by FD spectra, where the transitions in UV range at λ_{max} = 309 and 353 nm exhibit

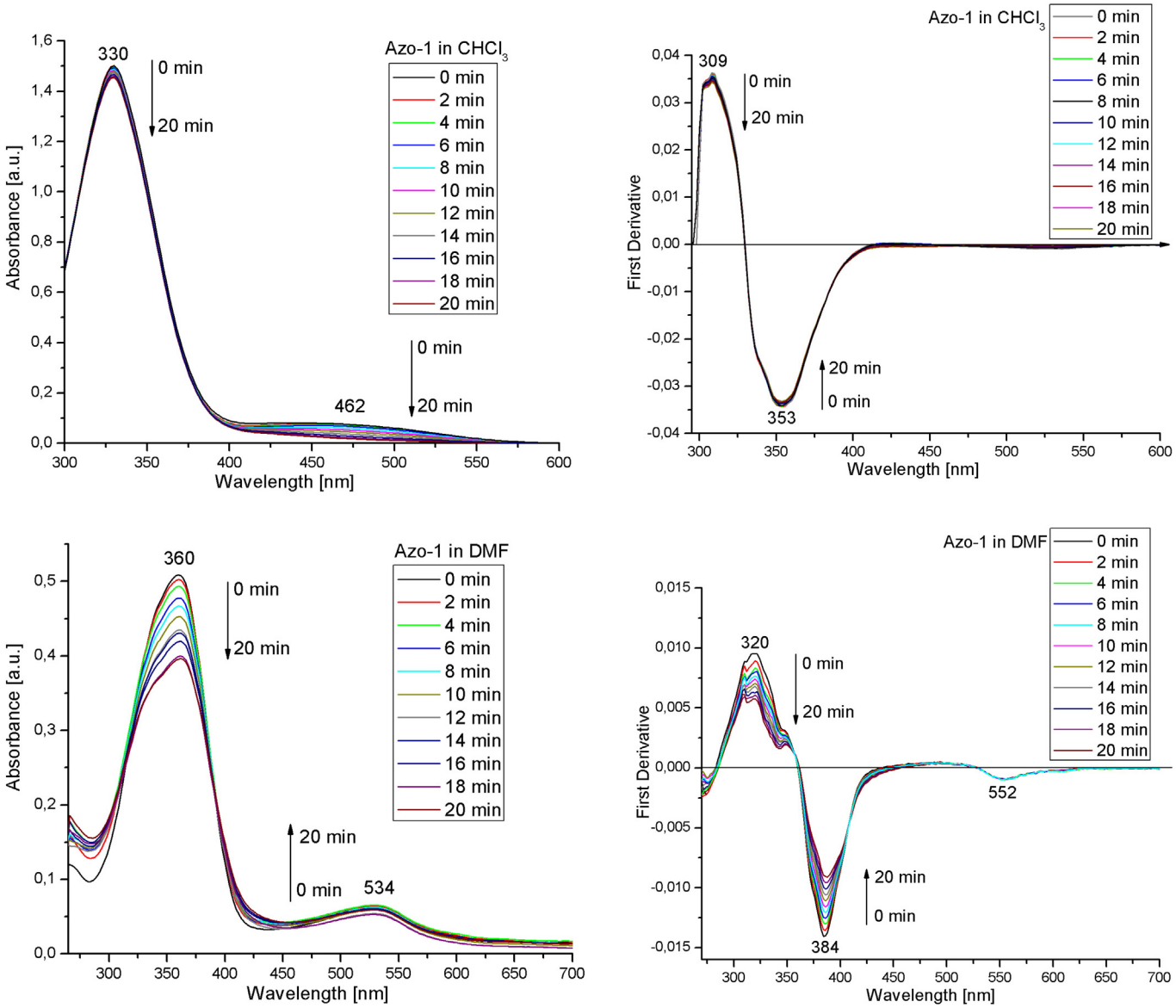

Fig. 9. Absorption and FD UV-VIS spectra of the photoisomerization experiment of Azo-1 in $CHCl_3$ and DMF performed by UV-irradiation with λ = 365 nm for 20 min.

no significant difference. In DMF solvent the n → π* (λ_{max} = 534 nm) absorption intensity increasing weakly with the illumination time, while for π → π* transition (λ_{max} = 360 nm) the decreased intensity of the absorbance band is considerable after 20 min period. The results are visualized from FD spectra at λ_{max} = 320 and 384 nm. For Azo-2 in $CHCl_3$ (Fig. 10) there was no isomerization, while in DMF a very small changes of the absorption bands at λ_{max} = 346, 397 and 533 nm are registered. The reasons might be: (i) the differences between lengths (*L*) of intramolecular hydrogen bonds of the *trans (E)* and *cis (Z)* isomers (Figs. 3 and 4) $\Delta L = L_{cis} - L_{trans}$ decrease in order: 0.065 Å (Azo-3) > 0.059 Å (Azo-2) > 0.026 Å (Azo-1). This means that Azo-2 has higher stability in *trans (E)* isomer compared to the Azo-1 (ii) steric effects of *ortho* —NO_2 group in *cis (Z)* isomer. This is confirmed by bigger C—N═N—C dihedral angle −17.86° compared to the Azo-1, −14.32° and Azo-3, −11.45°. (iii) fast reversible *trans-cis-trans* photoisomerization cycle; (iv) low intensity of the applied UV-light and short time of irradiation. After derivatization, the bands at λ_{max} = 326, 362, 420 and 572 nm are split. Interesting results are observed for Azo-3 in $CHCl_3$, where after 2 min period of irradiation the absorbance was decreased fast with bathochromic shift to λ_{max} = 391 nm (Fig. 11). After this period there were no significant absorption changes. The isomerization in DMF, after exposure for 2 min period the causes the absorption to decrease strongly without shifting. After this irradiation time, the absorption was changed evenly for 20 min period. The FD indicated well separated π → π* band at 389 nm and n → π* at 449 and 478 nm.

The electronic spectra of *trans (E)* and *cis (Z)* azo dyes calculated by TD-DFT after geometry optimization using IEFPCM in $CHCl_3$ and DMF are presented on Fig. 12. The electron transitions energy and molecular contributions of *trans → cis* are given in Supplementary information Tables S.10, S.11, S.12, S.13, S.14, S.15, S.16, S.17, S.18, S.19, S.20, S.21. The *trans (E)* isomers of Azo-1 and Azo-2 are characterized with strong absorption in visible region, which referred to the HOMO → LUMO and HOMO-1 → LUMO transitions. However, experimental UV-VIS spectra have shown weak absorption bands and oscillator strength (Table 5) in this range because of direct $S_0 \rightarrow S_1$ (n → π*) transitions are unlikely compared to the favorable $S_0 \rightarrow S_2$ (π → π*) transitions. It should be noted that the properties of single molecule are quite different from those when the molecules interacting each other. The π → π* bands in ultraviolet region are consist of several energetically close transitions with different molecular contributions: HOMO-2 → LUMO, HOMO → LUMO + 2 and HOMO-1 → LUMO + 1. This indicate that EW groups decrease the energy levels due to the conjugation on molecular backbones and intramolecular electron transfers. The spectra of *cis*

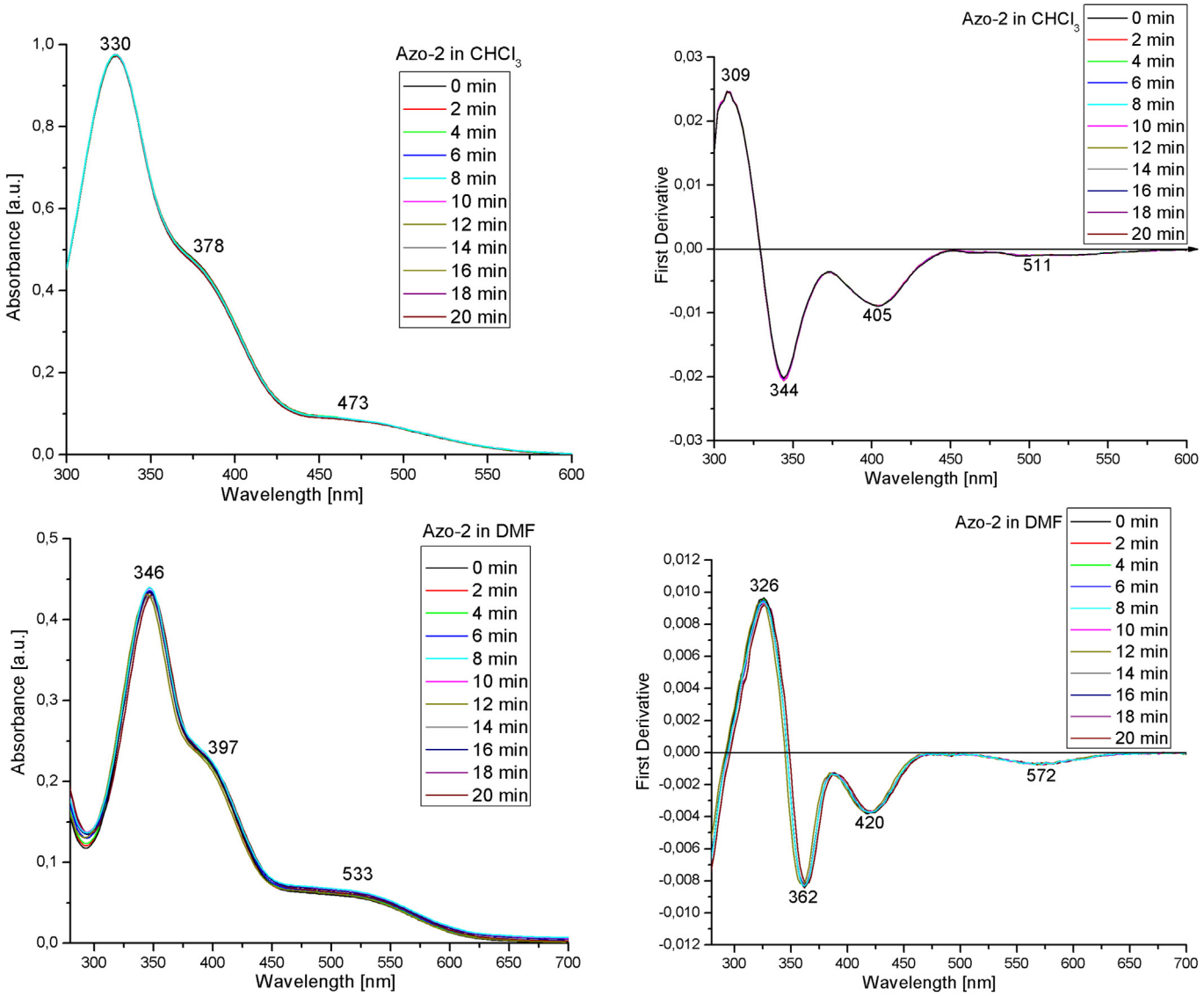

Fig. 10. Absorption and FD UV-VIS spectra of the photoisomerization experiment of Azo-2 in $CHCl_3$ and DMF performed by UV-irradiation with λ = 365 nm for 20 min.

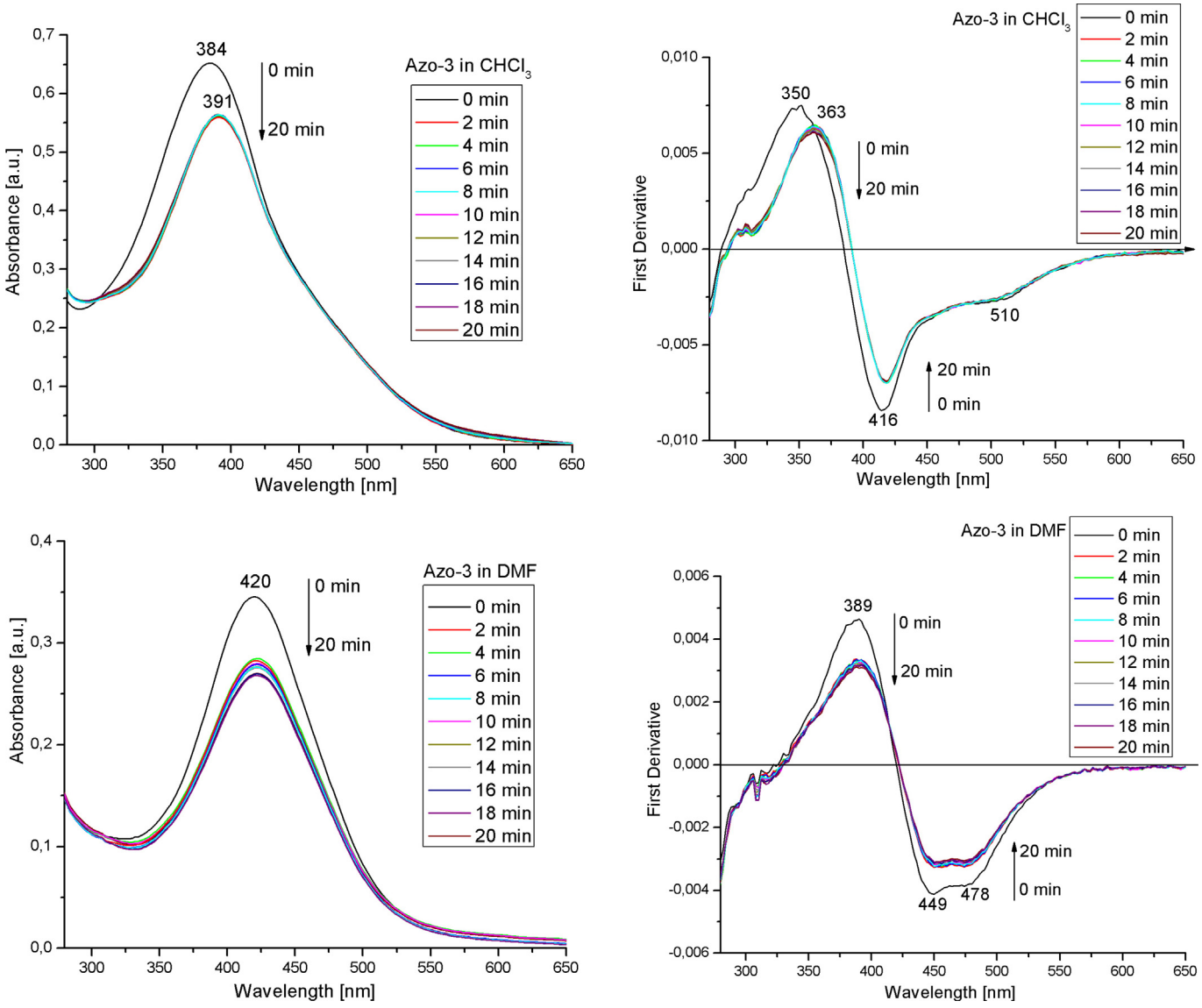

Fig. 11. Absorption and FD UV-VIS spectra of the photoisomerization experiment of Azo-3 in $CHCl_3$ and DMF performed by UV-irradiation with λ = 365 nm for 20 min.

(Z) isomers in $CHCl_3$ demonstrate forbidden HOMO-1 → LUMO (450 nm Azo-1) or weakly HOMO → LUMO + 2 (448 nm Azo-2) transitions in visible region, while in DMF the absorptions are increased. The results are in good agreement with experimental spectra, especially for Azo-1. Direct HOMO → LUMO is most likely transition of *trans (E)* Azo-3 in both solvents, which is in good agreement with experimental. Strong hypsochromic shift in *cis (Z)* isomer is observed related to the π → π* transition (HOMO-1 → LUMO) due to the loss of polarization (-I effect) of the Br atom and n-π conjugation of the —NH_2 group on molecular backbone. In general, strong EW groups in *ortho* and *para* positions increase the conjugation and energy levels on intramolecular electron transfers are decreased. The ED and EW with –I and +M effects give the direct HOMO → LUMO transition as main absorption band in visible range.

Table 6
Experimentally estimated values of the photoisomerization degree, R, in $CHCl_3$ and DMF.

Compounds	R	Compounds	R
	$CHCl_3$		*DMF*
Azo-1		Azo-1	
($\pi \rightarrow \pi^*$) λ_{max} = 330 nm	3.13	($\pi \rightarrow \pi^*$) λ_{max} = 360 nm	22.13
($n \rightarrow \pi^*$) λ_{max} = 462 nm	71.45	($n \rightarrow \pi^*$) λ_{max} = 534 nm	2.04
Azo-2	–	Azo-2	–
Azo-3		Azo-3	
($\pi \rightarrow \pi^*$) λ_{max} = 384 nm	14.12	($\pi \rightarrow \pi^*$) λ_{max} = 420 nm	21.86
($n \rightarrow \pi^*$)		($n \rightarrow \pi^*$)	

The presence of intramolecular hydrogen bond in the azo molecules allowed discussion on probable inversion mechanisms from *trans (E)* to *cis (Z)* isomerization, based on the quantum chemical calculations and photoisomerization experiment, where the —N(10)═N(11)—C(12) angle (114.70° for Azo-1) increases to 180° and dihedral angle remains fixed at 0°. The hydrogen bond occupies the nonbonding orbital (electron pair) of azo N(10) and the formed dipole compensate the electron density from neighboring N(11) (Fig. 5 and Table 3). For this reason the resonance electron distribution between —CH_2O—**H**···**N**═**N**—C is lower in energy compared to the non-hydrogen bonding. The rotation mechanism is unlikely due to the stability of hydrogen bonding on —N═N— group. The bond length of the *trans (E)* isomer —N(10)═N(11)— (for Azo-1 is 1.2785 Å) is shorter than ═N(11)—C(12) (for Azo-1 is 1.3968 Å) (Supplementary information Tables S.1, S.2 and S.3). In the *cis (Z)* isomer the resulting —N(10)═N(11)—C(12) angle is 126.10° (for Azo-1), the bond length between —N(10)═N(11)— is 1.2559 Å (for Azo-1) and ═N(11)—C(12) is 1.4120 Å. (Supplementary information Tables S.4, S.5 and S.6). The Azo-2 and Azo-3 have similar bond parameters.

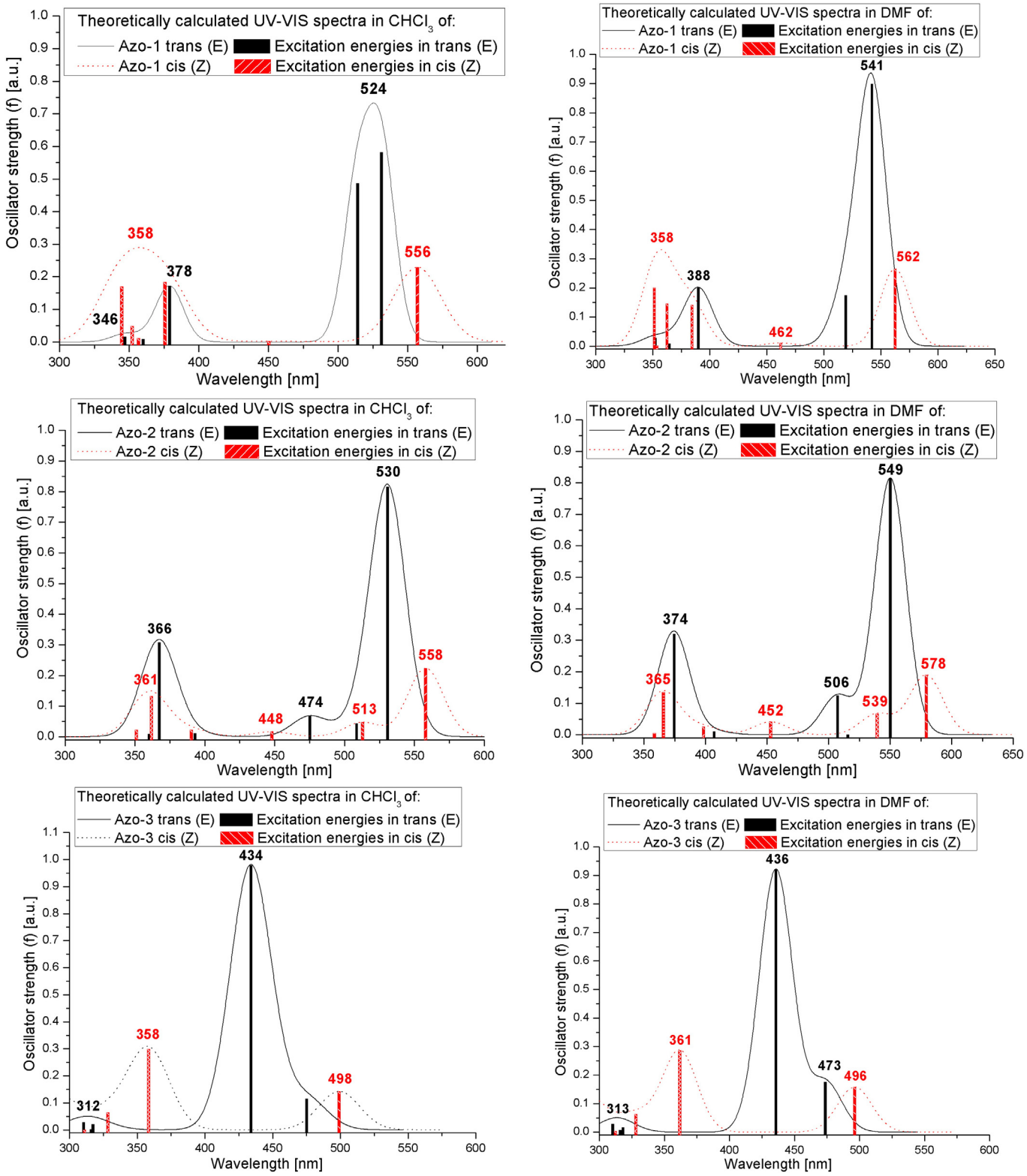

Fig. 12. Theoretically calculated UV-VIS spectra of the trans (E) and cis (Z) azo dyes by TD-DFT/B3LYP 6-31 + G(d,p) level of theory using IEFPCM in $CHCl_3$ and DMF solvents.

The absorption of the n → π* ($S_0 \rightarrow S_1$) transition in nonpolar $CHCl_3$ solvent is decreased during conversion from *trans (E)* to *cis (Z)* isomer due to the symmetry-forbidden transition and six-membered intramolecular hydrogen bonding [32]. Only in polar protic or aprotic solvents the absorption of n → π* transition is increased by photoisomerization, because of solvation the nonbonding electrons by dipole-dipole interactions with the solvents. The effect of intramolecular hydrogen bonding is not depending on the solvent properties, but only on the polarity and geometry of molecules. It should be noticed that phenol –OH group in *ortho* place to the azo group causes a strong azo-hydrazone tautomerism dependent on the solvent polarity. In our molecules such tautomerization is impossible because of the alkoxy anion is a strong base without possibility for resonance stabilization by conjugation to aromatic π electrons likewise the phenol —OH group [33]. The difference of tautomerization

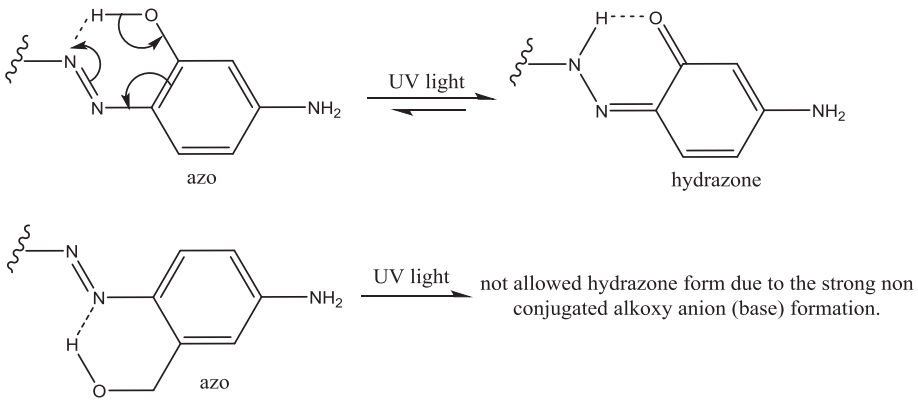

Scheme 2. Difference of azo-hydrazone tautomerization between phenol —OH and hydroxymethyl —CH_2OH groups.

between phenol —OH and hydroxymethyl —CH_2OH groups in *ortho* position to the azo group is illustrated on Scheme 2.

The intramolecular hydrogen bonds might be important from practical application point of view, because the photoisomerization can be driven by different intensities of the UV light in different polar media. Moreover, the *cis (Z)* isomer might be stabilized by intramolecular hydrogen bonding interaction and the reverse process to the *trans (E)* isomer can be driven easily by exposure to VIS light or thermal treatment. These could find an application in the optical photoswitches, optical storage information devices and solar cells.

4. Conclusions

Three 4-aminoazobenzene "push-pull" dyes (Azo-1, Azo-2 and Azo-3) with existing intramolecular hydrogen bond between the —CH_2OH and —N═N— groups have been synthesized. The optimized molecular geometry of *trans (E)* and *cis (Z)* isomers was computed at DFT/B3LYP 6-31 + G(d,p) level of theory in vacuo and solvation using IEFPCM in $CHCl_3$ and DMF solvents. The calculated thermodynamic parameters $\Delta E_{trans \rightarrow cis}$, $\Delta\mu_{trans \rightarrow cis}$, $\Delta H_{trans \rightarrow cis}$, $\Delta G_{trans \rightarrow cis}$ and $\Delta S_{trans \rightarrow cis}$ have shown that Azo-1 and Azo-2 are more stable in *trans (E)* isomers, while for Azo-3 the photoisomerization to *cis (Z)* isomer is favored by the kinetic factor. The energy levels of frontier HOMO and LUMO molecular orbitals and E_g (energy of optical band gap) were computed and experimentally estimated by cyclic voltammetry and UV-VIS spectroscopy. The E_g of Azo-1 and Azo-2 are close: 2.15 and 2.20 eV, which corresponds to the computed: 2.57 and 2.61 eV. The introduction of the EW or ED substituents was chosen at 2′- and 4′- position in the phenyl ring with respect to the —N═N— group. For Azo-1 a —C≡N group was introduced as an EW at 2′-position and a -NO_2 group as a second EW at 4′-position. Two well separated bands in UV (λ_{max} = 339 nm) and VIS (λ_{max} = 498 nm) range are registered in PMMA solid film. The characteristic absorption peaks of Azo-2 as thin film in the UV are λ_{max1} = 337 and λ_{max2} = 338 nm and VIS is λ_{max} = 493 nm, where two EA -NO_2 groups in 2′- and 4′- places were chosen. The Azo-3 was synthesized with ED groups in 2′-position of —CH_3 (+I effect) and 4′-place of —Br (–I and + M effects), where the π → π* and n → π* transitions are not separated in UV-VIS spectra (λ_{max} = 403 nm) due to the substituents properties.

The solvatochromism of Azo-1 and Azo-2 is about 11 nm bathochromic (red) shift when increasing the solvent polarity: $CHCl_3$ (nonpolar) < EtOH (polar protic) < DMF (polar aprotic). The solvatochromism of Azo-3 is less than that of Azo-1 and Azo-2. The photoisomerization of azo chromophores was investigated by UV-VIS spectroscopy in $CHCl_3$ and DMF solutions at room temperature with λ = 365 nm UV irradiation and light intensity 4 W at equal concentrations and irradiation time. The photoisomerization degree was calculated, where for Azo-1 in $CHCl_3$ the n → π* transition considerable decreases compare to the π → π* transition. In polar DMF the absorption of π → π* transitions decreases, whereas of n → π* transition increases slightly. The results were confirmed by TD-DFT calculation, where HOMO → LUMO electron transitions $S_0 \rightarrow S_1$ (n → π*) in *cis (Z)* isomers are decreased. Azo-2 did not isomerize at these conditions due to the steric effects of *ortho* -NO_2 group in *cis (Z)* isomer and bigger C—N═N—C dihedral angle compared to the Azo-1 and Azo-2. The photoisomerization of Azo-3 is characterized with fast decrease of the absorption after 2 min UV-irradiation. Based on the quantum chemical calculations, solvatochromic behavior and photoisomerization experiment probable inversion mechanisms from *trans (E)* to *cis (Z)* photoconversion can be suggested due to the existing intramolecular six-membered hydrogen bond.

Conflict of Interest

The authors declared that the article content has no conflicts of interest.

Acknowledgments

This work was financial supported by the Bulgarian National Scientific Fund project BG NSFB T02-27 of the Ministry of Education and Science, Bulgaria and Contract UCTM No. 11595. We also thank the Czech Science Foundation project No. 15-05095S. The authors gratefully acknowledge the MADARA (Modelling in ADvAnced Research Actions) cluster RNF01/0110 for computation of the molecules.

Appendix A. Supplementary Data

Supplementary data to this article can be found online at http://dx.doi.org/10.1016/j.saa.2016.12.005.

References

[1] H.M. Dhammika Bandara, S.C. Burdette, Photoisomerization in different classes of azobenzene, Chem. Soc. Rev. 41 (2012) 1809–1825, http://dx.doi.org/10.1039/C1CS15179G.
[2] K.G. Yager, C.J. Barrett, in: Y. Zhao, T. Ikeda (Eds.), Azobenzene Polymers For Photonic Applications, Book Chapter in Smart Light-Responsive Materials, John Wiley & Sons, Inc. 2009, pp. 1–27 ISBN: 978-0-470-17578-1.
[3] Y.M. Riyad, S. Naumov, J. Griebel, C. Elsner, R. Hermann, K.R. Siefermann, B. Abel, Optical switching of azophenol derivatives in solution and in polymer thin films: the role of chemical substitution and environment, American Journal of Nano Research and Application 2 (6–1) (2014) 39–52, http://www.sciencepublishinggroup.com/journal/paperinfo.aspx?journalid=226&doi=10.11648/j.nano.s.2014020601.16.
[4] E. Merino, M. Ribagorda, Control over molecular motion using the cis–trans photoisomerization of the azo group, Beilstein J. Org. Chem. 8 (2012) 1071–1090, http://dx.doi.org/10.3762/bjoc.8.119.
[5] H. Rau, in: Y. Zhao, T. Ikeda (Eds.), Photoreactive Organic Thin Films, Elsevier Sci Ltd 2002, pp. 3–48 ISBN:9780080479972.
[6] H. Rau, in: H. Duerr, H. Bouas-Laurent (Eds.), Photochromism: Molecules and Systems, Elsevier, Amsterdam 2003, pp. 165–192 Revised edn. ISBN:9780080538839.
[7] C.R. Crecca, A.E. Roitberg, Theoretical study of the isomerization mechanism of azobenzene and disubstituted azobenzene derivatives, J. Phys. Chem. A 110 (2006) 8188–8203, http://dx.doi.org/10.1021/jp057413c.

[8] T. Fujino, T. Tahara, Picosecond time-resolved Raman study of trans-azobenzene, J. Phys. Chem. A 104 (2000) 4203–4210, http://dx.doi.org/10.1021/jp992757m.
[9] T. Fujino, S.Y. Arzhantsev, T. Tahara, Femtosecond time-resolved fluorescence study of photoisomerization of trans-azobenzene, J. Phys. Chem. A 105 (2001) 8123–8129, http://dx.doi.org/10.1021/jp0110713.
[10] E. Schab-Balcerzak, H. Flakus, A. Jarczyk-Jedryka, J. Konieczkowska, M. Siwy, K. Bijak, A. Sobolewska, J. Stumpe, Photochromic supramolecular azopolyimides based on hydrogen bonds, Opt. Mater. 47 (2015) 501–511, http://dx.doi.org/10.1016/j.optmat.2015.06.029.
[11] H.-F. Qian, T. Tao, Y.-N. Feng, Y.-G. Wang, W. Huang, Crystal structures, solvatochromisms and DFT computations of three disperse azo dyes having the same azobenzene skeleton, J. Mol. Struct. 1123 (2016) 305–310, http://dx.doi.org/10.1016/j.molstruc.2016.06.042.
[12] W. Luoxin, J. Xu, H. Zhou, C. Yi, W. Xu, Cis–trans isomerization mechanism of 4-aminoazobenzene in the S_0 and S_1 states: a CASSCF and DFT study, J. Photochem. Photobiol. A Chem. 205 (2009) 104–108, http://dx.doi.org/10.1016/j.jphotochem.2009.04.014.
[13] B. Babur, N. Ertan, Part 1: synthesis and visible absorption spectra of some new monoazo dyes derived from ethyl 2-amino-4-(40-substitutedphenyl)thiophenes, Spectrochim. Acta A Mol. Biomol. Spectrosc. 131 (2014) 319–328, http://dx.doi.org/10.1016/j.saa.2014.04.042.
[14] A. Mahmood, M.H. Tahir, A. Irfan, A.G. Al-Sehemi, M.S. Al-Assiri, Heterocyclic azo dyes for dye sensitized solar cells: a quantum chemical study, Computational and Theoretical Chemistry 1066 (2015) 94–99, http://dx.doi.org/10.1016/j.comptc.2015.05.020.
[15] S.B. Novir, S.M. Hashemianzadeh, Density functional theory study of new azo dyes with different π-spacers for dye-sensitized solar cells, Spectrochim. Acta A Mol. Biomol. Spectrosc. 143 (2015) 20–34, http://dx.doi.org/10.1016/j.saa.2015.02.026.
[16] J.A. Gámez, A. Koslowski, W. Thiel, Enhanced E → Z photoisomerisation of 2-aminoazobenzene, RSC Adv. 4 (2014) 1886–1889, http://dx.doi.org/10.1039/c3ra45376f.
[17] M.J. Frisch, G.W. Trucks, H.B. Schlegel, G.E. Scuseria, M.A. Robb, J.R. Cheeseman, G. Scalmani, V. Barone, B. Mennucci, G.A. Petersson, H. Nakatsuji, M. Caricato, X. Li, H.P. Hratchian, A.F. Izmaylov, J. Bloino, G. Zheng, J.L. Sonnenberg, M. Hada, M. Ehara, K. Toyota, R. Fukuda, J. Hasegawa, M. Ishida, T. Nakajima, Y. Honda, O. Kitao, H. Nakai, T. Vreven, J.A. Montgomery Jr., J.E. Peralta, F. Ogliaro, M. Bearpark, J.J. Heyd, E. Brothers, K.N. Kudin, V.N. Staroverov, R. Kobayashi, J. Normand, K. Raghavachari, A. Rendell, J.C. Burant, S.S. Iyengar, J. Tomasi, M. Cossi, N. Rega, J.M. Millam, M. Klene, J.E. Knox, J.B. Cross, V. Bakken, C. Adamo, J. Jaramillo, R. Gomperts, R.E. Stratmann, O. Yazyev, A.J. Austin, R. Cammi, C. Pomelli, J.W. Ochterski, R.L. Martin, K. Morokuma, V.G. Zakrzewski, G.A. Voth, P. Salvador, J.J. Dannenberg, S. Dapprich, A.D. Daniels, O. Farkas, J.B. Foresman, J.V. Ortiz, J. Cioslowski, D.J. Fox, Gaussian 09, Revision A.02, Gaussian, Inc., Wallingford CT, 2009.
[18] http://cccbdb.nist.gov/vibscalejust.asp.
[19] I.H.I. Habib, S.A. Weshahy, S. Toubar, M.M.A. El-Alamin, "Cathodic stripping voltammetric determination of Losartan in bulk and pharmaceutical products", Portugalie, Electrochim. Acta 26 (2008) 315–324, http://dx.doi.org/10.4152/pea.200804315.
[20] S. Georgieva, P. Todorov, D. Wesselinova, Synthesis, characterization and cytotoxic activity of novel Cu(II) and Co(II) complexes with 3-amino-5.5-dimethylhydantoin, Comptes Rendus Chimie 17 (2014) 1212–1220, http://dx.doi.org/10.1016/j.crci.2014.01.020.
[21] A. Cooksy, Physical Chemistry: Quantum Chemistry and Molecular Interactions, Chapter 7,8,9 Pearson Education, January 2013 ISBN-10: 0321814169.
[22] P. Govindasamy, S. Gunasekaran, Quantum mechanical calculations and spectroscopic (FT-IR, FT-Raman and UV) investigations, molecular orbital, NLO, NBO, NLMO and MESP analysis of 4-[5-(4-methylphenyl)-3-(trifluoromethyl)-1H-pyrazol-1-yl] benzene-1-sulfonamide, J. Mol. Struct. 1081 (2015) 96–109, http://dx.doi.org/10.1016/j.molstruc.2014.10.011.
[23] R.P. Gangadharan, S. Sampath Krishnan, Natural bond orbital (NBO) population analysis of 1-azanapthalene-8-ol, Acta Phys. Pol. A 125 (1) (2014) 18–22, http://dx.doi.org/10.12693/APhysPolA.125.18.
[24] L. Leonat, G. Sbârcea, I.V. Brânzoi, Cyclic voltammetry for energy levels estimation of organic materials, U.P.B. Sci. Bull., Series B 75 (3) (2013) 111–118 ISSN 1454-2331.
[25] J.L. Bredas, R. Silbey, D.S. Boudreux, R.R. Chance, Chain-length dependence of electronic and electrochemical properties of conjugated systems: polyacetylene, polyphenylene, polythiophene, and polypyrrole, J. Am. Chem. Soc. 105 (1983) 6555–6564, http://dx.doi.org/10.1021/ja00360a004.
[26] C. Ye, M. Li, J. Luo, L. Chen, Z. Tang, J. Pei, L. Jiang, Y. Song, D. Zhu, Photo-induced amplification of readout contrast in nanoscale data storage, J. Mater. Chem. 22 (2012) 4299–4305, http://dx.doi.org/10.1039/C2JM14923K.
[27] S.N. Inamdar, P.P. Ingole, S.K. Haram, Determination of band structure parameters, and quasiparticle gap of CdSe quantum dots by cyclic voltammetry, ChemPhysChem 9 (2008) 2574–2579, http://dx.doi.org/10.1002/cphc.200800482.
[28] S. Seridi, K. Dinar, A. Seridi, M. Berredjem, M. Kadri, Charge transfer complexes of 4-isopropyl-2-benzyl-1,2,5-thiadiazolidin-3-one1,1-dioxide with DDQ and TCNE: experimental and DFT studies, New J. Chem. 40 (2016) 4781–4792, http://dx.doi.org/10.1039/C5NJ03017J.
[29] L. Zheng, N.F. Polizzi, A.R. Dave, A. Migliore, D.N. Beratan, Where is the electronic oscillator strength? Mapping oscillator strength across molecular absorption spectra, J. Phys. Chem. A 120 (11) (2016) 1933–1943, http://dx.doi.org/10.1021/acs.jpca.6b00692.
[30] A. Airinei, N. Fifere, M. Homocianu, C. Gaina, V. Gaina, B.C. Simionescu, Optical properties of some New Azo photoisomerizable bismaleimide derivatives, Int. J. Mol. Sci. 12 (2011) 6176–6193, http://dx.doi.org/10.3390/ijms12096176.
[31] S. Kus, Z. Marczenko, N. Obarski, Derivative UV-VIS spectrophotometry in analytical chemistry, Chem. Anal. 41 (1996) 899–927.
[32] Ian Fleming. Molecular Orbitals and Organic Chemical Reactions. Chapter, 1, 2, 6, 8, John Wiley & Sons Inc. Reference Edition 2010, ISBN 978-0-470-74660-8.
[33] A. Ünal, B. Eren, E. Eren, Investigation of the azo-hydrazone tautomeric equilibrium in an azo dye involving the naphthalene moiety by UV–vis spectroscopy and quantum chemistry, J. Mol. Struct. 1049 (2013) 303–309, http://dx.doi.org/10.1016/j.molstruc.2013.06.037.